DOI:10.14753/SE.2025.3240

SEMMELWEIS EGYETEM

DOKTORI ISKOLA

Ph.D. értekezések

3240.

SZÁSZ ADRIENN ZSÓFIA

A gyógyszerészeti tudományok korszerű kutatási irányai

című program

Programvezető: Dr. Antal István, egyetemi tanár

Témavezető: Dr. Kőhidai László, egyetemi tanár
Dr. Lajkó Eszter, egyetemi docens

DOI:10.14753/SE.2025.3240

IN VITRO EVALUATION OF SMALL MOLECULES AND PEPTIDE-BASED CONJUGATES FOR TARGETED TUMOUR THERAPY IN PANCREATIC TUMOUR CELL LINES

PhD thesis

Adrienn Zsófia Szász, PharmD

Pharmaceutical Sciences and Health Technologies Program

Semmelweis University

Supervisor: László Kőhidai, MD, Ph.D

Eszter Lajkó, PharmD, Ph.D

Official reviewers: Zelles Tibor, MD, Ph.D

Lilla Turiák, PharmD, Ph.D

Head of the Complex Examination Committee: István Antal, PharmD, Ph.D

Members of the Complex Examination Committee:

Tibor Gergely Kozma, Ph.D

Krisztina Ludányi, Ph.D

Budapest

2025

DOI:10.14753/SE.2025.3240

Table of Contents

DOI:10.14753/SE.2025.3240

List of abbreviations

7AAD	7-aminoactinomycine
Akt	Protein kinase B
ANOVA	one-way analysis of variance
Apaf-1	apoptotic protease activating factor 1
ATF4	activating transcription factor 4
BRCA	Breast Cancer gene
BOZ	bortezomib
CAF	cancer-associated fibroblasts
CAR T-cell	chimeric antigen receptor T-cell
CCNA1	Cyclin A1
CCND2	Cyclin D2
CCNE1	Cyclin E1
CDC25A	Cell Division Cycle 25A
CDC25C	Cell Division Cycle 25C
CDKN1A	Cyclin Dependent Kinase Inhibitor 1A, p21
CI	Cell Index
cIAP-1	Cellular Inhibitor of Apoptosis Protein 1
ClpP	caseinolytic protease P
Dau	Daunorubicin
dCK	deoxycytidine kinase
dFdC	difluorodeoxycytidine
DMSO	dimethyl sulfoxide
DR4	death receptor 4
DR5	death receptor 5
E2F1	E2F Transcription Factor 1
E2F2	E2F Transcription Factor 2
E2F3	E2F Transcription Factor 3
ECACC	European Collection of Authenticated Cell Cultures

EMT	epithelial-mesenchymal transition
Erk	extracellular signal-regulated kinase
FADD	Fas-associated death domain
Fisher's LSD	Fisher's Least Significant Difference
FITC	fluorescein isothiocyanate
FOXO3a	forkhead box O3
GAPDH	glyceraldehyde-3-phosphate dehydrogenase
GLB1	β-galactosidase
hCNT	human concentrative nucleoside transporter
hENT	human equilibrative nucleoside transporter
HPRT1	hypoxanthine phosphoribosyltransferase
HSP60	Heat shock protein 60
IC50	half-maximal inhibitory concentration
KRAS	Kristen rat sarcoma viral oncogene homolog
LDH	lactate dehydrogenase
LGALS3	galectin 3
NHDF	normal human dermal fibroblasts
PARP	Poly (ADP-ribose) polymerase
PBS	phosphate buffered saline
PDAC	pancreas ductal adenocarcinoma
PDC	peptide-drug conjugate
PI	Propidium iodide
RRM1	ribonucleotide reductase M1
RRM2	ribonucleotide reductase M2
ROS	reactive oxygen species
SMAC	second mitochondria-derived activator of caspases
TBP	TATA-box binding protein
TERT	telomerase reverse transcriptase
TIC-10	TRAIL inducing compound 10

TME	tumour microenvironment
TP53BP1	p53 binding protein 1
TRAIL	TNF-related apoptosis-inducing ligand
XIAP	X-linked inhibitor of apoptosis protein

DOI:10.14753/SE.2025.3240

1. Introduction

1.1. Pancreas ductal adenocarcinoma

Pancreas ductal adenocarcinoma (PDAC) is amongst the cancers with the highest mortality rates, and researchers predict the prevalence will rise even more in the future (1). Despite some improvement, the 5-year survival rate remains low at 11% and is strongly influenced by the operability of the tumour (2). This low survival rate is due to late-stage diagnosis, often after metastasis has occurred, and the tumour's poor response to chemotherapy, coupled with frequent development of resistance (3, 4). To make matters worse, it is still unclear in detail which cellular mechanisms are involved in tumorigenesis. Hence, understanding the cellular origins of PDAC remains a focal point of research. However, there is consensus that PDAC often harbours *KRAS* (Kristen rat sarcoma virus) gene mutations and that pancreatic intraepithelial neoplasia may be a potential precursor state (4, 5). Additionally, several chronic diseases, for example, diabetes mellitus and lifestyle factors, including smoking and alcohol consumption, heighten the risk of developing PDAC (1). Current treatment for PDAC depends mainly on the resectability of the tumour. If the tumour is operable, surgery is the first choice, often followed by adjuvant chemotherapy (6). However, most cases are unsuitable for surgery, and these patients receive chemotherapy or palliative care. The gold standard for treating PDAC is gemcitabine, either as monotherapy or in combination with other cytotoxic agents. Another option is the combinational therapy FOLFIRINOX, which includes folinic acid (a vitamin B derivative), 5-fluorouracil, irinotecan and oxaliplatin. Unfortunately, these therapies have limited efficacy, as reflected in the low 5-year survival rates. In 2019, the FDA approved olaparib for treating *BRCA* (Breast cancer gene)-mutated PDAC patients, making it the only targeted therapy available (7). This highlights a significant gap in effective treatment options. Another promising option for treating PDAC could be personalized therapies, such as CAR (chimeric antigen receptor) T-cell therapy, which is a highly researched area in oncology (8). However, many studies indicate that CAR T-cell therapy is not suitable for PDAC due to the high amount of stromal cells, which form a dense physical barrier; therefore, the immune cells can not enter

the tumour site (9). By addressing these challenges, researchers hope to develop more effective treatments and improve outcomes for PDAC patients.

1.1.1. Gemcitabine resistance

Resistance to chemotherapy presents a significant challenge in the treatment of PDAC patients. Chemoresistance to gemcitabine is particularly significant because it is a prodrug that requires activation to exert its anti-tumour effect. Through enzymatic modifications, gemcitabine (difluorodeoxycytidine, dFdC) is turned into its active form, difluorodeoxycytidine triphosphate (10). The active compound then inhibits DNA synthesis and initiates apoptotic cell death. However, chemoresistance can easily develop due to both extrinsic and intrinsic factors within the tumour microenvironment (TME). One of the key features of PDAC is its high cellular heterogeneity and the presence of numerous stromal cells, particularly cancer-associated fibroblasts (CAFs), which form a dense barrier around the tumour (Figure 1). This physical barrier hinders the effectiveness of chemotherapy by preventing gemcitabine from entering the cancer cells, leading to the development of extrinsic resistance (11). Moreover, the CAFs can compress the vessels around the tumour, generating hypoxia that alters the metabolism of the tumour cells (12). This will cause a higher amount of lactate in the extracellular matrix, which causes a drop in pH levels (Figure 1). A lower pH level is more favourable for the epithelial-mesenchymal transition (EMT) of the cancer cells, which also affects the uptake of the compound (13). In addition, the influence of stromal cells can also cause intrinsic resistance by altering the function of transporters responsible for gemcitabine uptake, such as the human equilibrative nucleoside transporter (hENT) and the human concentrative nucleoside transporter (hCNT). The expression of hENT changes under EMT-induced hypoxia, reducing the number of active transporters in the plasma membrane (14). Stromal cells can also modify cancer cell metabolism, inhibiting drug activation through two mechanisms: (1) downregulating the expression of deoxycytidine kinase (dCK), the enzyme responsible for converting gemcitabine into the monophosphate form (the most crucial step in the activation), or (2) upregulating the expression of ribonucleotide reductase M1/M2 (RRM1/RRM2) enzymes, which enhances the nucleoside pool by supplying deoxynucleotides, thereby reducing gemcitabine's efficacy (15). To address these issues, researchers are focusing on strategies that target

the TME to reduce chemoresistance and increase the efficacy of gemcitabine (16). Although this approach looks promising, the development of novel therapeutic approaches for PDAC patients remains crucial.

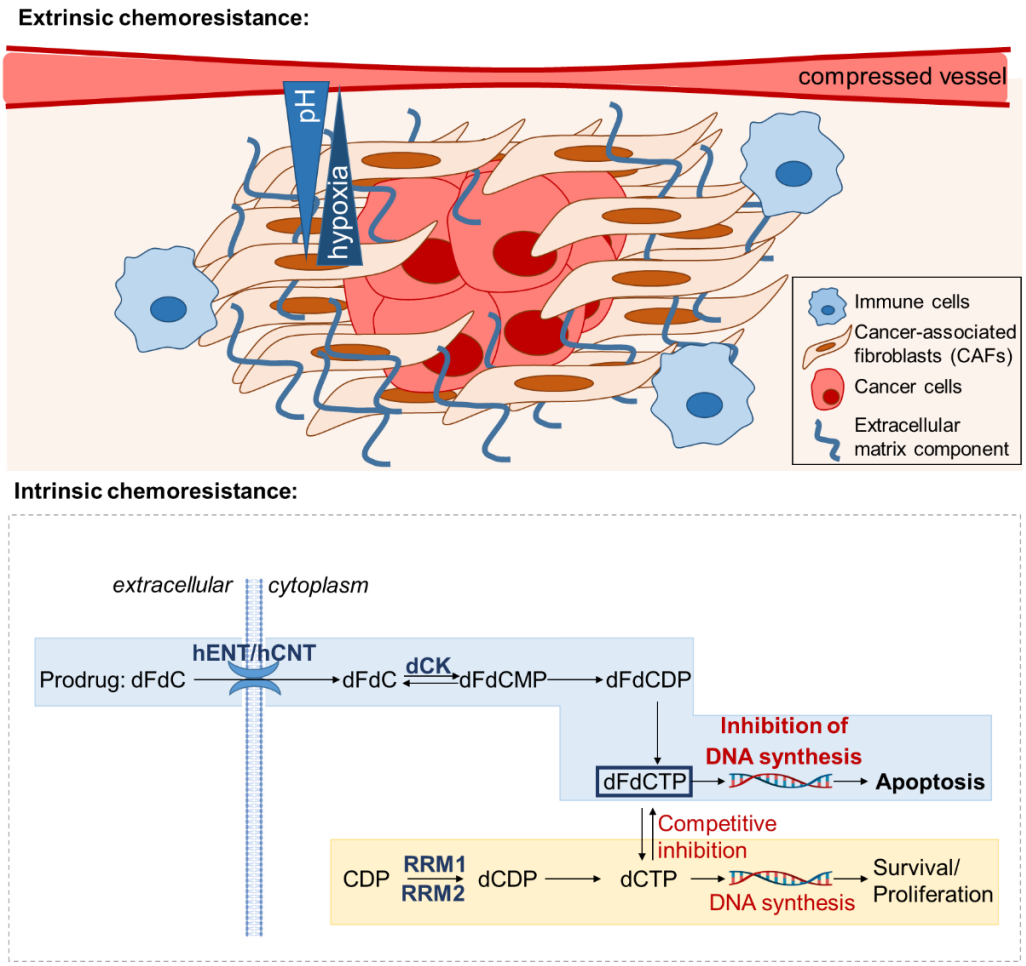

Figure 1. A graphical representation of the extrinsic and intrinsic factors contributing to chemoresistance. Highlighting the role of the tumour microenvironment, particularly cancer-associated fibroblasts (CAFs), in drug transport inhibition, hypoxia-induced metabolic changes, and altered drug activation pathways. The abbreviations found on the figure: dFdC – difluorodeoxycytidin, hENT/hCNT - human equilibrative/ concentrative nucleoside transporter, dCK - deoxycytidine kinase, dFdCMP - difluorodeoxycytidine monophosphate, dFdCDP - difluorodeoxycytidine diphosphate, dFdCTP - difluorodeoxycytidine triphosphate – active form, CDP - cytidine diphosphate, RRM1/RRM2 - ribonucleotide reductase M1/M2, dCDP - deoxycytidine diphosphate, dCTP - deoxycytidine triphosphate. The figure is adapted from the figure found in this paper (17).

1.2. Targeted therapies

Targeted therapies have long been desired for patients with PDAC, as they offer the hope of a more effective form of treatment with fewer side effects. These agents can be divided into two main groups: small molecules and macromolecules/biologics. Despite numerous clinical trials aimed at developing targeted treatments, only one agent is currently in clinical use: olaparib. Olaparib is a PARP (poly (ADP-ribose) polymerase) inhibitor that is effective in patients with a *BRCA* mutation (18). While *BRCA* mutations are common in ovarian and breast cancer patients, their incidence in PDAC is relatively low. Approximately 10% of familial PDAC cases and only 3% of sporadic PDAC cases carry the mutation (19). This low prevalence means that the majority of PDAC patients will not be able to benefit from this targeted therapy, highlighting a significant limitation in the current targeted treatment landscape.

1.2.1. Small molecules

One class of molecules that can be used for targeted therapy is the so-called small molecules. The main characteristics of these compounds are low molecular weight (<900 Da), favourable pharmacokinetic profile, low cost, good patient adherence and easier storage compared to macromolecules (20). Several drugs belong to this group, which are already in clinical use. The most known are the protein kinase inhibitors, which are used in the treatment of several tumours. For example, imatinib is a Bcr-Abl tyrosine kinase inhibitor used most commonly in chronic myeloid leukaemia (21, 22).

1.2.1.1. ONC201/ TIC-10

In the last decade, a novel antitumour molecule family was developed, which is the imipridones. Among them is ONC201, also referred to as the TRAIL (TNF-related apoptosis ligand)-inducing compound 10 (TIC-10). ONC201 has emerged as a promising small molecule agent investigated in numerous clinical trials as a targeted anti-tumour drug (23, 24). Its mechanism of action, well-documented in recent studies, involves triggering apoptosis through both the extrinsic and intrinsic pathways (Figure 2) (25, 26). The activation of the extrinsic pathway occurs through the upregulation of TRAIL by inhibiting the Akt (protein B kinase) and Erk

(extracellular signal-regulated kinase) pathways. Through the activation of the transcription factor FOXO3a (forkhead box O3), the transcription of TRAIL is upregulated. After the enhanced protein synthesis, TRAIL can be found in membrane-bound and soluble forms. The membrane-bound form of the protein can cause a supra-molecular clustering upon binding to the death receptors, which results in an enhanced apoptotic signal (27). Moreover, Monleón et al. reported that overactivated T-lymphocytes secrete TRAIL in a membrane-bound form of extracellular vesicles (28). After the enhanced transcription of TRAIL, the protein binds to its receptors, death receptor 4/5 (DR4, DR5) and initiates the caspase cascade and subsequent apoptotic cell death. ONC201 also enhances TRAIL expression in NK cells, facilitating their recruitment to the tumour sites. This effect has been supported by studies by Wagner et al., which have demonstrated the efficacy of ONC201 in reducing the size of tumours *in vivo* (29). Simultaneously, ONC201 directly binds to its target, the mitochondrial caseinolytic protease P (ClpP), a serine protease enzyme, activating the intrinsic apoptotic pathway through the activating transcription factor 4 (ATF4) in a p53-independent manner (30). However, ONC201 causes cell cycle arrest, which can also induce the intrinsic pathway of apoptosis in a p53-dependent manner (31). This results in cytochrome C release from the mitochondria and the assembly and subsequent apoptosome activation, followed by the initiation of the caspase cascade. This process is p53-dependent, while the extrinsic and the ATF4-mediated intrinsic apoptotic pathway is p53-independent. It is beneficial that ONC201 can simultaneously activate both apoptotic pathways because PDAC usually harbours *TP53* mutation, which causes the dysfunction or total loss of p53 (32).

DOI:10.14753/SE.2025.3240

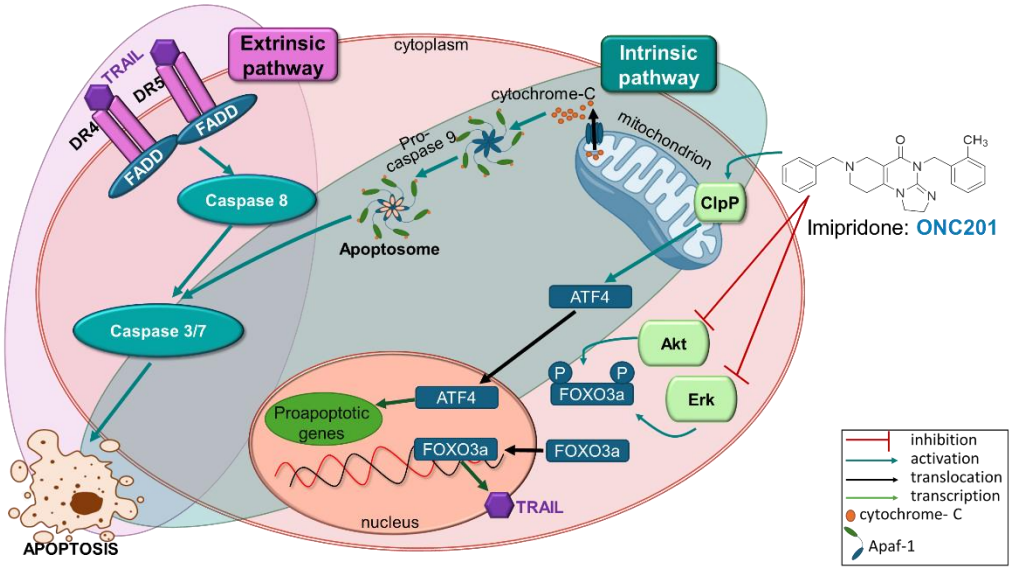

Figure 2. A schematic diagram illustrating ONC201's mechanism of action. The extrinsic pathway is triggered by the upregulation of TRAIL via inhibition of Akt and Erk signalling, leading to increased TRAIL expression. TRAIL then binds to death receptors DR4 and DR5, initiating the caspase cascade. Simultaneously, ONC201 activates the intrinsic pathway p53-idependetly through ClpP and ATF4. The abbreviations found in the figure: ClpP - caseinolytic protease P, TRAIL - TNF-related apoptosis-inducing ligand, DR4 - death receptor 4, DR5 - death receptor 5, FADD - Fas-associated death domain, Akt - protein kinase B, Erk - extracellular signal-regulated kinase, FOXO3a - forkhead box O3a, ATF4 - activating transcription factor 4, Apaf-1 - apoptotic protease activating factor 1.

1.2.1.2. Combinational therapy with ONC201

The use of combinations of cytotoxic drugs in oncotherapy is a well-developed strategy to improve treatment efficacy and patient outcomes (33). By targeting multiple pathways simultaneously, these combinations can enhance therapeutic effects, overcome drug resistance, and reduce toxicity through dose optimisation. Zhang et al. have already reported that ONC201 could enhance the sensitivity of PANC-1 cells to gemcitabine (25). This suggests that it may have the ability to act synergistically with other cytotoxic agents and broaden the range of available combinational treatments for other cancer types.

1.2.2. Peptide-drug conjugates

Peptide-drug conjugates (PDC) are an emerging opportunity for targeted therapy. PDCs can serve as an alternative to antibody-drug conjugates and can be produced more cost-effectively. The peptides in PDCs are synthesised using the solid phase peptide synthesis method, which is an *in vitro* technology (34). Therefore, the peptide-drug conjugates are not considered as biologics. For this reason and because of their size, these molecules are less likely to be immunogenic compared to antibodies or antibody-drug conjugates (35). PDCs are usually built up from a pharmacologically active agent, e.g. cytotoxic drug molecule, which is conjugated to a targeting peptide. The composition can be altered, and a linker sequence can be inserted between the drug and the targeting peptide. The linker sequence helps to stabilise the PDC in the bloodstream by preventing premature drug release but can promote the liberation of the drug or its pharmacologically active metabolite from the conjugate inside the target cells (36). The targeting sequence is the key to personalising these PDCs in a clinical setting. The peptides specific to a given tumour can be selected based on known molecular markers of the target tumour cells, or they can be selected based on the result of the phage display library (37, 38). Despite the diverse and promising drug delivery systems that PDCs represent, currently, none are in clinical use. Earlier, there were attempts at clinical use, such as Zoptrex™ (Zoptarelin Doxorubicin, AEZS-108, AN-152), a drug consisting of an anthracycline, doxorubicin, conjugated to a GnRH analogue peptide via a glutaric acid spacer, developed for GnRH receptor-positive cancers (e.g. endometrial and ovarian adenocarcinoma) (39). Despite optimistic expectations, the PDC failed to pass the phase III clinical trial due to the lack of improvement in median overall survival compared to the unconjugated doxorubicin (40).

1.2.2.1. Daunorubicin & Daunorubicin-based peptide conjugates

Daunorubicin (Dau), a well-established cytotoxic agent belonging to the anthracycline family, is commonly used in the treatment of leukaemias (41). It works by inhibiting topoisomerase II in the dividing cancer cells, therefore disrupting the cell cycle and ultimately promoting apoptotic cell death. Despite its long history of clinical use, Dau is known to induce severe cardiotoxicity due to the lack of tumour

selectivity (42). However, for a long time, researchers were unsure about what causes the severe side effect, the answer was found in the last decade. There are two main pathways that contribute to the cardiotoxic side effect, both involving mitochondrial function: (a) topoisomerase IIβ-dependent and (b) topoisomerase IIβ-independent (43). The non-dividing cardiomyocytes express topoisomerase IIβ isoform in their mitochondria, where Dau can inhibit the activity of the enzyme, causing enhanced reactive oxygen species (ROS) production (44). In addition, the molecule can directly bind to cardiolipin in the inner mitochondrial membrane, disrupting the electron transport chain and generating an excessive amount of ROS. Furthermore, Zhan et al. reported that the high amount of ROS production is mainly caused by the inhibition of topoisomerase IIβ, while the electron transport chain had a lesser impact on the generation of excessive ROS (45). In order to improve selectivity and lessen the cardiotoxicity, Dau can be conjugated with peptides. As a form of PDC, Dau can be targeted precisely to tumour cells by recognising cell surface molecule(s) specific for tumour cells (46). Moreover, the targeting sequence of PDCs can be easily tailored to a specific type of tumour, increasing the selectivity and effectiveness of the Dau-based treatment.

What mechanisms enable the Dau-containing PDC to enter tumour cells and exert its therapeutic effects? Firstly, the PDC containing Dau binds to the target receptor on the surface of the tumour cell. Then, the receptor-PDC complex is internalised, presumably through receptor-mediated endocytosis, which is a selective uptake process (Figure 3) (47). Next, the PDC detaches from the receptor in the early endosome. The next step, depending on the linker sequence, is its enzymatic cleavage by the lysosomal enzyme cathepsin B. Then the active metabolite of Dau linked to the remaining amino acids (depending on the linker sequence) can leave the lysosome and enter the nucleus. Upon entering the nucleus, it can inhibit DNA synthesis by blocking topoisomerase II. This will result in cell cycle arrest and, ultimately, apoptotic cell death.

DOI:10.14753/SE.2025.3240

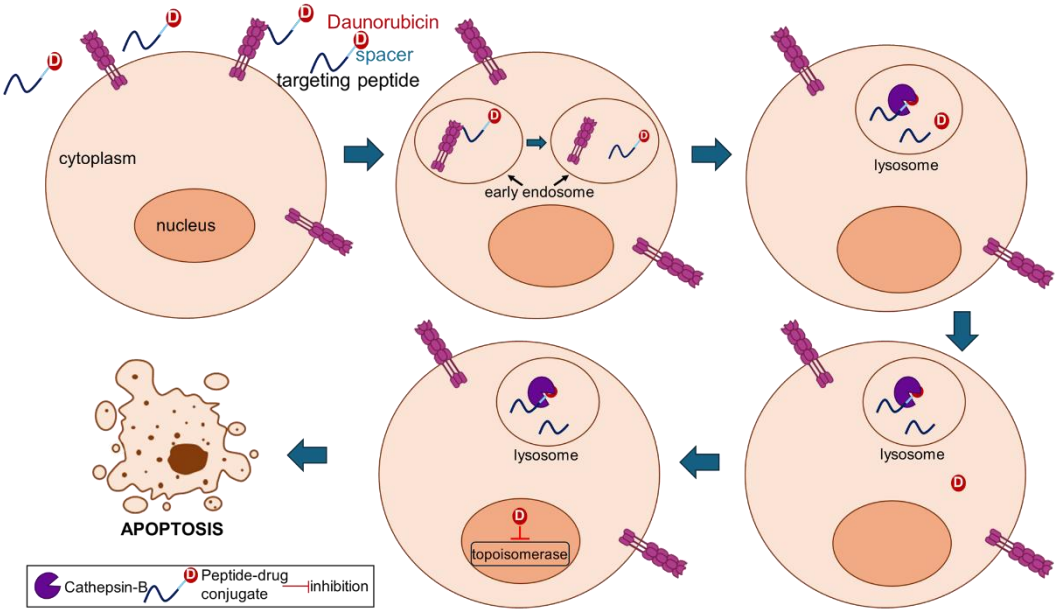

Figure 3. The schematic figure of the cellular uptake and the mechanism of action of daunorubicin-peptide conjugates. After binding to tumour-specific receptors, the complex is internalised via receptor-mediated endocytosis, followed by enzymatic cleavage in the lysosome. The released active metabolite enters the nucleus, where it inhibits topoisomerase II, leading to cell cycle arrest and apoptosis.

1.3. Halogenation in drug development

Halogenation is a commonly used technique in medicinal chemistry for drug discovery and development (48). This process enhances the interaction between drugs and their targets, influencing both the pharmacokinetic and pharmacodynamic profiles of medications. Halogen atoms, due to their unique electronic properties, can significantly alter the biological activity of a molecule, often leading to improved efficacy, selectivity and metabolic stability. For example, fluorination has been shown to significantly enhance p53 activation (49). Fluorine's small size and high electronegativity make it a valuable addition to drug molecules, often increasing their binding affinity to biological targets and resistance to metabolic degradation (50).

Chlorination, another form of halogenation, can be used as an alternative to fluorination due to their similar electron-withdrawing properties (51). Chlorine, being larger than fluorine, can cause different steric effects and modulate the lipophilicity of the compound, which may enhance its ability to cross cell membranes or improve

its distribution in tissues (52). This versatility in halogenation allows for the fine-tuning of drug properties to optimise therapeutic outcomes.

DOI:10.14753/SE.2025.3240

2. Objectives

In my PhD work, studies focused on characterising the anti-tumour effects of halogenated derivatives. First, we examined small molecules, specifically the meta- and para-fluorinated analogues of ONC201, to understand the importance of fluorination in enhancing the pharmacological activity of these compounds. To understand the effect of these molecules a PDAC cell line (PANC-1) was used. In addition, the molecular background of the synergistic effect of ONC201 with bortezomib was revealed on metastatic melanoma cells (A2058).

2.1. In vitro characterisation of the mechanism of action of ONC201 and its halogenated analogues

a. Do the analogues have anti-tumour effects on the tumour cell line, and do they have a direct cytotoxic effect on PANC-1 cells?
b. Do they influence the cell cycle of PANC-1 cells?
c. Do they induce apoptotic cell death in PANC-1 cells?
d. Are they able to induce the level of TRAIL in PANC-1 cells?
e. What is the molecular background of their supposed apoptosis-inducing effect in PANC-1 cells?
f. Determination of molecular background underlying the synergistic effect of ONC201 and bortezomib on metastatic melanoma, A2058 cell line. Do the combination of ONC201 and bortezomib increase the expression of the death receptors?

The second part of my thesis describes the effect of modifying the targeting sequence of the Dau-peptide conjugates with a non-natural amino acid (e.g. halogenated amino acid) on the viability and cell death of PANC-1 cells.

2.2. Investigation of the cell and molecular biological effect of Dau-based peptide conjugates in vitro.

a. Do the conjugates have anti-tumour effects on the tumour cell line, and to what extent can the PANC-1 cells uptake the conjugates?
b. Do they have a direct cytotoxic effect on PANC-1 cells?
c. How can they mediate their anti-tumour effect on PANC-1 cells?
d. Do they have cardiotoxic effects in vitro in the long term?

DOI:10.14753/SE.2025.3240

3. Methods

3.1. Cell culturing

Two tumour cell lines (pancreas adenocarcinoma, PANC-1 and metastatic melanoma, A2058) were used in our experiments to evaluate the effects of the investigated molecules on cell physiological parameters. To test the cardiotoxicity of the tested conjugates, an immortalised mouse cardiomyocyte cell line (HL-1) was used. The immortalised mouse cardiomyocyte cells (HL-1) were cultured in coated cell flasks with 0.02% gelatine (Sigma Ltd. St. Louis, MO, USA) solution containing 5 μg/mL fibronectin (Merck, Darmstadt, Germany). To investigate the tumour selectivity of the ONC201 derivates, normal human dermal fibroblast cells (NHDF) were used. The cells and their culturing media are included in Table 1.

Table 1. Cell lines and their culturing media

Cell line	Basal Medium	Supplemented with
pancreas adenocarcinoma, PANC-1 (87092802 ECCAC)	DMEM (Lonza Group AG, Basel, Switzerland)	10% FCS (Biosera, Nuaille, France), 1% penicillin/ streptomycin (Sigma Ltd. St. Louis, MO, USA), 1% L-glutamine (Lonza Group AG, Basel, Switzerland)
metastatic melanoma, A2058 (91100402 ECCAC)	RPMI (Lonza Group AG, Basel, Switzerland)	
NHDF (Promocell, Heidelberg, Germany)	Fibroblast Growth Medium (Promocell, Heidelberg, Germany)	Supplement Mix (Promocell, Heidelberg, Germany)
HL-1 (Merck, Darmstadt, Germany, Lot: RD1601001, SCC065)	Claycomb (Merck, Darmstadt, Germany)	10% FCS, 1% penicillin/ streptomycin, 1% L-glutamine, 1% noradrenaline (Sigma Ltd. St. Louis, MO, USA, 100x stock in 30 mM L-ascorbic acid)

3.2. Materials

The ONC201 and its analogues were synthesized by Professor Antal Csámpai and Péter Bárány, and the peptide conjugates were prepared by Professor Gábor Mező and Nóra Kata Enyedi at the Institute of Chemistry, Faculty of Science, Eötvös Lóránd University, and were kindly provided to us for testing. The stock solutions (Table 2.) were aliquoted and stored at -80°C, and fresh dilutions were prepared using a complete cell culture medium for each experiment.

Table 2. Materials

Substance	**Solvent**	**Concentration of stock solution (mM)**
peptide conjugates	distilled water	5
ONC201 and its analogues	DMSO	10
bortezomib (Velcade 3.5 mg; Janssen-Cilag GmbH, Neuss, Germany)	distilled water	30

Cell culture medium and, in the case of ONC201 and its analogues, DMSO (<1 v/v%) were used as controls in both viability experiments and all the subsequent measurements. The experiments were carried out in triplicates unless otherwise stated, and the results were normalised to either the medium or the DMSO (<1 v/v%) control.

3.3. Viability assay

In the case of ONC201 and its derivates, the aim of the cell viability measurements was to determine the half-maximal inhibitory concentration (IC_{50}) value at which the treatment reduced the cell viability to 50% compared to the control-treated samples. We have tested the molecules in a 2-fold dilution series ranging from 50 μM to 250 nM.

For testing the cell viability after treatment with Dau and the peptide conjugates, three different concentrations (1, 10 and 100 μM) were used.

3.3.1. xCELLigence

The xCELLigence SP (Roche Applied Science, Indianapolis, IN, USA) device works based on impedimetric and real-time measurement techniques (53). The effects of the molecules on the viability of PANC-1 cells were determined using this system. Firstly, a baseline was obtained with a cell-free culture medium for 1 hour at 1-minute intervals. Then, the cells (10^4 cells/well) were added to the so-called E-plate and cell adhesion was assessed for 24 hours at 15-minute time points. After 24 hours, the investigated compounds were added to the system, and the changes in impedance were monitored for 96 hours. The Cell Index (CI) was used to express the changes in impedance as a relative and dimensionless parameter and was recorded every 5 minutes for 24 hours and then every 15 minutes for 72 hours.

3.3.2. AlamarBlue

The AlamarBlue assay was used to measure the viability of NHDF cells. First, the cells were plated on a 96-well culture plate at $2.5x10^3$ cells/well/200 µL concentration. Following 24 hours of cultivation, the cells were treated with the tested compounds. After 24, 48, and 72 hours of treatment AlamarBlue (0.15 mg/mL resazurin, Thermo Fisher Scientific, Waltham, MA, USA) was added to the cells, and after 5 hours of incubation with the dye, the fluorescent intensity of the samples was measured (λ_{ex}: 530-560 nm, λ_{em}: 590 nm) with the Fluoroskan FL fluorimeter (Thermo Scientific, Waltham, MA, USA).

3.3.3. CellTiter Glo - Cardiotoxicity

In order to determine the cardiotoxic effects of Dau and the peptide conjugates, the CellTiter Glo Luminescent Cell Viability Assay (Promega, Madison, WI, USA) was used to measure the viability of HL-1 cells. Cells were seeded on a white 96-well plate with optical bottom at $4x10^4$ cells/well/100 µL. When the spontaneous pacemaker activity of the cells started, after 72 hours of culturing, 100 µL fresh media was added and then treated the cells with the conjugates (ConjA, Conj03 and Conj16) at 1, 10 and 100 µM concentrations for 72 hours. After the 72-hour treatment, half of the supernatant (100 µL) was carefully discarded, and an equivalent amount of CellTiter Glo solution was pipetted to the wells. Then, we followed the manufacturer's instructions and the Fluoroskan FL fluorimeter (Thermo Scientific, Waltham, MA, USA) was used to measure the luminescence.

3.4. Apoptosis assay

To determine the number of cells in the early- and late apoptotic stages a double labelling method was used for flow cytometric analysis. Annexin-V FITC (Sony Biotechnology, Weybridge, UK) was used to detect the phosphatidylserine in the outer plasma membrane, which is one of the early markers of apoptosis (54, 55). The other labelling molecules were specific DNA dyes that can help determine the membrane integrity of the cells (56). In the case of ONC201 and its derivates, 7AAD (7-Aminoactinomycin D, Sony Biotechnology, Weybridge, UK) was used, and after treatment with Dau and the peptide conjugates, To-Pro^{TM}3 (Invitrogen Corporation, New York, NY, USA) was used (57, 58).

The preparation of the samples after treatment with Dau and the conjugates was described in great detail in this paper (59). In the case of treatment with ONC201 and its analogues, the cells were treated at concentrations of 0.5, 10 and 25 μM for 24-, 48- and 72 hours. The cells were prepared the same as described in the paper only difference was that instead of To-Pro^{TM}3 Ready Flow^{TM} Reagent 7AAD was used as the DNA dye. BD FACSCalibur (Becton–Dickinson, San Jose, CA, USA) was used for the flow cytometric analysis, and a minimum of 10000 cells/sample were measured. The data was evaluated using Flowing Software 2.5.1 (Turku Centre of Biotechnology, Turku, Finland).

3.5. Cell cycle analysis

To analyse the cell cycle, the DNA content of cells was measured with a flow cytometer (BD FACSCalibur, Becton–Dickinson, San Jose, CA, USA) using propidium iodide (PI), the fluorescent DNA intercalating dye (60). The preparation of the samples and the data evaluation are very similar to those described in this paper (61). First, the cells were plated in 24-well culture plates at 2x10^4 cells/well /450 μL. After 24 hours of cultivation, the cells were treated with 0.5 μM ONC201 and its derivates. After 48- and 72-hour treatment, the cells were prepared as described in the paper by Lajkó et al. (61), and the cells were resuspended in 70% ethanol at -20℃ and incubated for 30 min at room temperature, followed by an additional 24-hour incubation at -20℃. Then, to remove the ethanol, the cells were centrifuged for 5 min (300 g). Subsequently, the cells were resuspended in citric acid/ disodium hydrogen phosphate buffer (pH=7.8) containing 100 μg/mL RNase A (Sigma Ltd. St. Louis,

MO, USA). 6 µL of PI (Sony Biotechnology, Weybridge, UK) was added immediately before measurement to each sample. In each case, a minimum of 25,000 cells/sample were measured during the flow cytometric (BD FACSCalibur, Becton–Dickinson, San Jose, CA, USA) analysis, and 2 parallel samples were analysed. To evaluate the results, Flowing Software 2.5.1 (Turku Centre of Biotechnology, Turku, Finland) was used.

3.6. Direct cytotoxicity assay

The CyQuant^{TM} LDH Cytotoxicity Assay (Invitrogen Corporation, New York, NY, USA) was used to determine the direct cellular cytotoxicity of the investigated compounds (62). Sample preparation and data evaluation are similar to those described in our previous work (63). Firstly, the cells were seeded in a 96-well plate at 10^4 cells/well/200 µL, and after 24 hours of cultivation, the cells were treated with the molecules. 50 µL of the media from each well was pipetted into a new 96-well plate after 48 and 72 hours of treatment. The assay was then performed according to the manufacturer's manual. The absorbance was measured for each well at 492 and 680 nm using a plate reader (Multiskan MS, Labsystems, Helsinki, Finland). The '% cytotoxicity' was then calculated according to the manufacturer's instructions.

3.7. Tracking of the morphological changes

A holographic transmission microscope (HoloMonitor M4; Phase Holographic Imaging AB, Lund, Sweden) was used to track the morphometric changes of the cells. This microscope uses a laser to produce hologram or pseudo-3D images of the cells using the phase shift from the sample beam and the reference beam (64, 65). This method allows us to detect the cells in real time, label-free. First, the cells were seeded at $3.5x10^5$ cells/flask/4000 µL, and after 24 hours of seeding, the cells were treated with the compounds. After 24-, 48- and 72-hour treatment, at least 5 images were taken from each culture dish, making sure to assess different fields of view. During the image analysis three parameters (cells' average area, optical thickness and optical volume) were tracked and analysed by the built-in software (Hstudio M4, Phase Holographic Imaging AB, Lund, Sweden). For the analysis, a minimum of 25 cells were identified in each image using the minimum error histogram-based threshold algorithm in the software.

3.8. Caspase 3/7 detection

CellEvent™ Caspase-3/7 Green Detection Reagent (ThermoScientific, Waltham, MA, USA) was used to assess caspase-3/7 activity and imaging was performed using the ZEISS Celldiscoverer 7 (Carl Zeiss AG, Jena, Germany). Cells were initially plated at a density of 10^4 cells/well/200µL in black 96-well plates with an optical bottom. After 24 hours of incubation, the cells were treated with ONC201 and TBP-135 at concentrations of 0.5, 10 and 25 µM. CellEvent™ Caspase-3/7 reagent was then added, and measurements were performed according to the manufacturer's protocol. A kinetic setup was used to monitor changes in the number of caspase-3/7 positive cells over time. Imaging was performed using the Celldiscoverer 7 with one position per well, maintaining the same field of view for each well at each time point. Samples were imaged using 5× Plan-Apochromat 5×/0.35 NA objective with a 2× tube lens (Carl Zeiss AG, Oberkochen, Germany), capturing images in brightfield (exposure time: 10 ms) and the FITC channel (λ_{ex}: 495 nm, λ_{em}: 519 nm, exposure time: 500 ms). Image analysis was performed using ZEN Blue 2.6 software (Carl Zeiss AG, Oberkochen, Germany).

3.9. Apoptotic protein analysis

The apoptotic protein profile of the treated PANC-1 cells was measured using the Human Apoptosis Array Kit (R&D Systems, Minneapolis, MN, USA), which determines the expression of 35 apoptosis-related proteins. The total protein content was isolated from the cells after a 72-hour treatment with ONC201 and its derivates at a concentration of 0.5 µM. One confluent culture dish ($1{,}5x10^6$ cells/flask) was used for protein isolation for each treatment group. The total protein concentration was measured using the Micro BCA Protein Assay Kit (Thermo Scientific, Waltham, MA, USA) according to the manufacturer’s protocol. The Human Apoptosis Array Kit was used to establish the apoptotic protein profile. For this, 225 µg of protein was added to the membranes, and the required steps were carried out in accordance with the manufacturer's instructions. The Bio-Rad Chemidoc XRS+ instrument (BIO-RAD, USA) was used to take images of the membranes and images were analysed using ImageLab software (BIO-RAD, USA).

3.10. Gene expression analysis

First, PANC-1 cells were seeded at a concentration of $0.5x10^6$ cells/well/1800 µL in a 6-well plate, and A2058 cells were seeded at a concentration of $1x10^6$ cells/flask/5000 µL. After 24 hours of seeding, the PANC-1 cells were treated with the conjugates at a concentration of 10 µM or with ONC201 and its analogues at 25 µM. The A2058 cells were treated with 13.5 and 40.5 µM ONC201, 13.5 nM bortezomib and with their combinations: 13.5nM Bortezomib + 13.5 µM ONC201, 13.5nM Bortezomib + 40.5 µM ONC201. The total RNA was isolated using the RNeasy kit (Qiagen, Hilden, Germany) according to the manufacturer's manual. The concentration of the RNA was measured using the NanoDrop-1000 spectrophotometer (Thermo Fisher Scientific, Waltham, MA, USA). RNA was then reverse transcribed into cDNA at a concentration of 1000 ng/20 µL using the SensiFAST^{TM} cDNA synthesis kit (Bioline Reagents Ltd., London, UK). For the amplification, the Sso Advanced Universal SYBR Green Supermix (BioRad, Hercules, CA, USA) was used in 20 µL for the 96-well PCR plate or 10 µL final volume for the 384-well PCR plate. The measurement was performed using the CFX96 or CFX384 TouchTM Real-Time PCR system with the BioRad CX Maestro software (BioRad, Hercules, CA, USA). For the same target genes, three technical replicates were measured with all the samples, and 'no template' controls (NTC) were used for each primer. To calculate the changes in gene expression, the $2^{-(\Delta\Delta Ct)}$ method was used (66). Upregulation was considered biologically significant with at least a 2-fold change, while downregulation was defined as at least a 0.5-fold change (67).

3.10.1. Apoptotic genes

To determine the effect of bortezomib and ONC201 and their combinations on the expression of death receptors in A2058 cells, *DR4* and *DR5* at mRNA level was determined after 72-hour treatment. To test the effects of ONC201 and its analogues on the apoptotic gene expression of PANC-1 after 3-, 6-, 12-, 24-, and 48-hour treatment, 4 target genes were selected: *DR4* and *DR5*, *p53* and *TRAIL.* They were chosen based on our apoptotic protein profiling results and the literature on the mechanism of action of ONC201.

We used pre-designed gene-specific primers, which were the following: DR4 (*TNFRSF10A*, unique assay ID: qHsaCID0018590); DR5 (*TNFRSF10B,* unique assay

ID: qHsaCED0036477); p53 (*TP53*, unique assay ID: qHsaCED0045022); TRAIL (*TNFSF10*, unique assay ID: qHsaCED0036477); glyceraldehyde-3-phosphate dehydrogenase (*GAPDH*, unique assay ID: qHsaCED0038674); TATA-box binding protein (*TBP*, unique assay ID: qHsaCID0007122), hypoxanthine phosphoribosyltransferase (*HPRT1*, unique assay ID: qHsaCID0016375). The housekeeping genes were used for normalisation, in A2058 cells *GAPDH* and *HPRT1* genes, in PANC1 cells *GAPDH* and *TBP* were selected.

3.10.2. Senescence-related genes

First, the changes in the expression of 88 genes were screened using a predesigned 96-well panel of cellular senescence markers (Cellular senescence (SAB Target List) H96, BioRad, Hercules, CA, USA). In this screening, a 48-hour treatment of 10 μM Conj16, the most effective conjugate, was studied on PANC-1 cells. 14 genes (β-galactosidase (*GLB1*, unique assay ID: qHsaCID0012007); p21 (*CDKN1A*, unique assay ID: qHsaCID0014498); p53 (*TP53*, unique assay ID: qHsaCED0045022); p53 binding protein 1 (*TP53BP1*, unique assay ID: qHsaCID0020917); E2F1 (*E2F1*, unique assay ID: qHsaCID0016226); E2F2 (*E2F2*, unique assay ID: qHsaCID0022067); E2F3 (*E2F3*, unique assay ID: qHsaCID0009515); telomerase reverse transcriptase (*TERT*, unique assay ID: qHsaCID0009247); Cyclin A1 (*CCNA1*, unique assay ID: qHsaCID0008934); Cell Division Cycle 25A (*CDC25A*, unique assay ID: qHsaCID0036715); Cell Division Cycle 25C (*CDC25C*, unique assay ID: qHsaCED0045810); Cyclin D2 (*CCND2*, unique assay ID: qHsaCID0011859); Cyclin E1 (*CCNE1*, unique assay ID: qHsaCID0015131); galectin 3 (*LGALS3*, unique assay ID: qHsaCED0044416); TATA-box binding protein (*TBP*, unique assay ID: qHsaCID0007122)) were selected for further analysis and comparison of the effect of the three selected conjugates (ConjA, Conj03, Conj16) based on the results of the senescence-related genes' expression (ΔCt).

To normalise the data, *TBP* was used as a housekeeping gene.

3.11. Cellular uptake of the peptide-drug conjugates

To determine the cellular uptake of the Dau-peptide conjugates to PANC-1 cells, a Cytoflex flow cytometer (Beckman Coulter, Indianapolis, IN, USA) was used (68, 69). The sample preparation and data evaluation are quite similar to those described in this paper (70). First, the cells were seeded at $2x10^5$ cells/well/900 µL concentration in a 12-well plate, and after 24 hours of cultivation, the cells were treated with Dau (0.5, 1 µM) and with the conjugates at 10 µM. The cells were then incubated for 1 hour at 37 °C and 4 °C simultaneously. Next, the cells were prepared, as described in this paper (59). During the flow cytometric analysis, a minimum of 20,000 cells/sample were measured using the phycoerythrin (PE) channel (λex: 561 nm, λem: 585 nm) The CytExpert Software (Beckman Coulter, Indianapolis, IN, USA) was used for data evaluation. The quantification of the relative amount of the conjugates taken up by the cells is provided in this paper (59).

3.12. Statistical Analysis

The data presented in the Results section - mean ± SD of parallel measurements - were statistically evaluated using Origin Pro8.0 software (OriginLab Corporation, Northampton, MA, USA). The IC_{50} value was calculaed by plotting the viability values of the molecules used as a function of log concentrations, fitting a curve to the points (Sigmoidal Fitting/Dose Response Curves).To analyse the significance of the data, a one-way analysis of variance (ANOVA, *post hoc* test: Fisher's LSD) was used. Levels of significance were indicated as follows: x - $p<0.05$; y - $p<0.01$; z - $p<0.001$.

DOI:10.14753/SE.2025.3240

4. Results

4.1. The effect of the small molecule, ONC201 and its fluorinated analogues

4.1.1. The fluorinated analogues have a reduced IC50 on PANC-1 cells and spare the healthy NHDF cells.

The viability measurements aimed to determine the IC_{50} values. After 24 and 48 hours of treatment, no viability-reducing effect was detected for any compounds (Figure 4A). In the case of ONC201, the IC_{50} value after 72-hour treatment was 6.1 μM (Figure 4A). With the introduction of fluorine into the demethylated ONC201 structure (TBP-134, TBP-135), the IC_{50} value significantly decreased to 0.35 and 1.8 μM, respectively.

Nevertheless, neither molecule exhibited a direct cytotoxic effect at 0.5 and 10 μM on PANC-1 cells. However, only the treatment with the highest concentration, 25 μM TBP-134, increased the direct cytotoxicity from 5.3% (Medium and DMSO control) to 6.9% (by 1.3-fold), which showed statistical significance. However, this rise can be considered biologically negligible. The other two molecules had no such effect (Figure 4B).

DOI:10.14753/SE.2025.3240

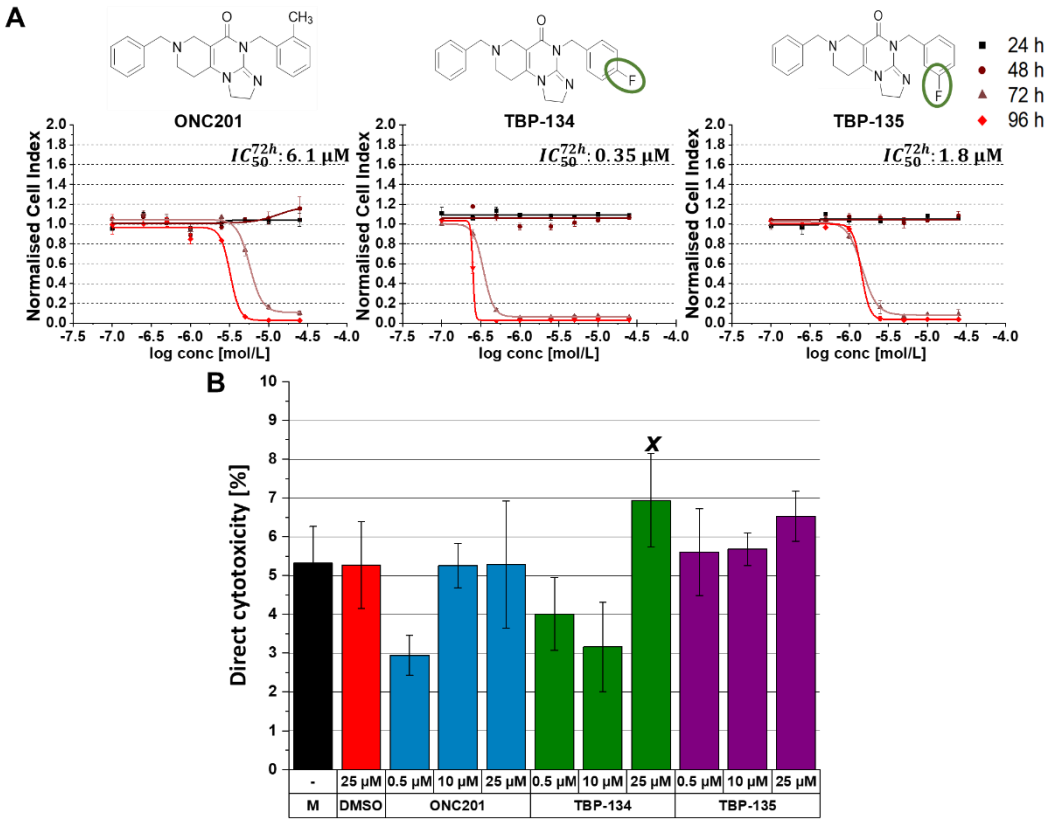

Figure 4. The analogues exhibit lower IC_{50} values against PANC-1 cells, and neither molecule shows direct cytotoxicity to PANC-1 cells at 0.5 µM. (A) The molecular structure and the dose-response curve of ONC201, TBP-134 and TBP-135 on PANC-1 cells. (B) The following formula was used to determine the direct cytotoxicity (%) of the molecules: $cytotoxicity\% = \frac{LDH\ activity_{treated} - LDH\ activity_{spontaneous}}{LDH\ activity_{maximum} - LDH\ activity_{spontaneous}}$ x 100 and was compared to the DMSO control. The data are presented as mean values ± standard deviation (SD) (n = 3). A one-way ANOVA test followed by Fisher's LSD *post hoc* test was used and the levels of significance are shown as x - $p<0.05$. The abbreviation n.d. stands for not detectable, while the M stands for medium control (71).

To determine the tumour-selective effect of the molecules, the viability of NHDF cells was measured. Although no significant antiproliferative effect was detected on NHDF cells at the IC50 concentrations determined in PANC-1 (Figure 5), all three molecules reduced the viability of NHDF cells at least an order-of-magnitude higher concentrations.

DOI:10.14753/SE.2025.3240

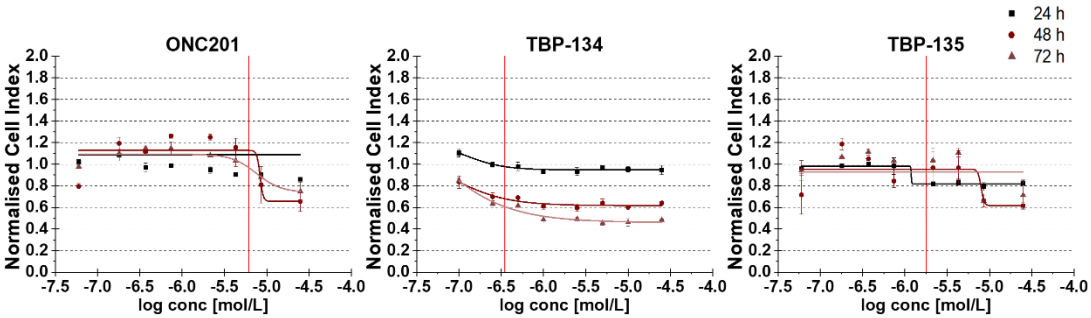

Figure 5. Neither molecule has measurable IC_{50} values against NHDF cells. Dose-response curve of ONC-201, TBP-134 and TBP-135 on NHDF cells. The data were normalised to the DMSO control wells. The red lines indicate the respective IC_{50} concentrations measured on PANC-1 cells. The data are presented as mean values ± standard deviation (SD) (n = 3). A one-way ANOVA test followed by Fisher's LSD *post hoc* test was used, and the levels of significance are shown as x - $p<0.05$ (71).

4.1.2. TBP-134 arrests the cell cycle of PANC-1 cells in the G2/M phase

After 48 hours of treatment with 0.5 μM TBP-134, a G2/M phase arrest was detected, which can be seen as a significant increase in the relative cell numbers in the G2/M phase, coupled with a significant reduction in the G1 phase (Figure 6A). G1 phase arrest was detected after treatment with 0.5 μM TBP-135, as the proportion of G1-phase cells increased. However, ONC201 did not affect the cell cycle at this time and concentration. After 72 hours of treatment with TBP-134, similar tendencies were observed, with a slightly enhanced effect (Figure 6B). While TBP-135 and ONC201 influenced the cell cycle similarly after 72 hours, promoting the G1 phase arrest. Interestingly, the proportion of the sub-G1 phase, which indicates the population of apoptotic bodies with DNA fragments formed during apoptosis, did not increase significantly in either case.

DOI:10.14753/SE.2025.3240

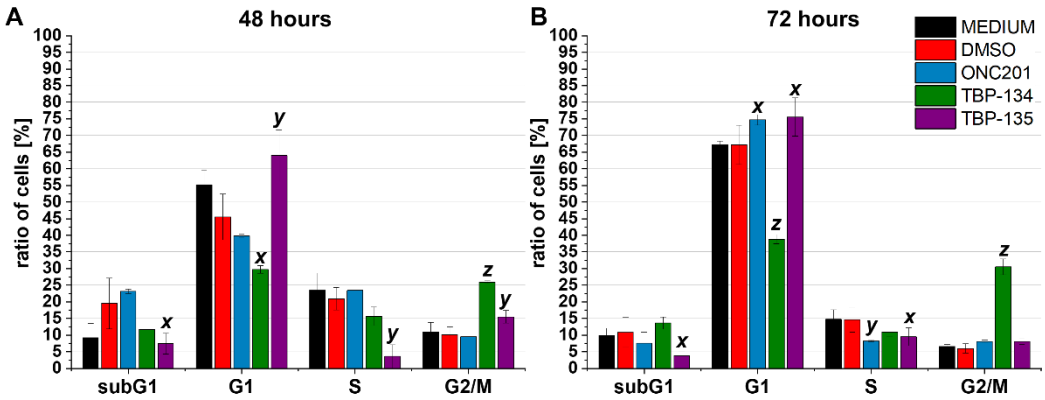

Figure 6. A 48-hour treatment with 0.5 µM TBP-134 causes a G2/M phase block in PANC-1 cells. Cell distribution in cell cycle phases is shown after (B) 48 and (C) 72 hours of treatment with the compounds at 0.5 µM. The data are presented as mean values ± standard deviation (SD) (n=2). Significance levels are calculated to the DMSO control and shown as x - $p<0.05$; y - $p<0.01$; z - $p<0.001$ using a one-way ANOVA test followed by Fisher's LSD *post hoc* test (71).

4.1.3. ONC201 and its analogues induce apoptosis

The apoptosis-inducing effect was the most pronounced in the case of 72 hours of treatment, where 0.5 µM TBP-134 and TBP-135 could significantly increase the ratio of early apoptotic cells (DMSO control: 21.1%) to 43.8% (by 2.1-fold) and 53.5% (by 2.5-fold), respectively (Figure 7A). The ratio of late apoptotic cells (AnnexinV positive and 7AAD positive population) was affected most after 72 hours. The two analogues at 0.5 µM also statistically significantly but slightly increased (DMSO control: 0.9%), TBP-134 could increase it to 3.8% (by 4.2-fold) and TBP-135 to 3.2% (by 3.5-fold) (Figure 7B). In contrast, even after 72 hours exposure to ONC201 did not induce apoptosis at the lowest concentration.

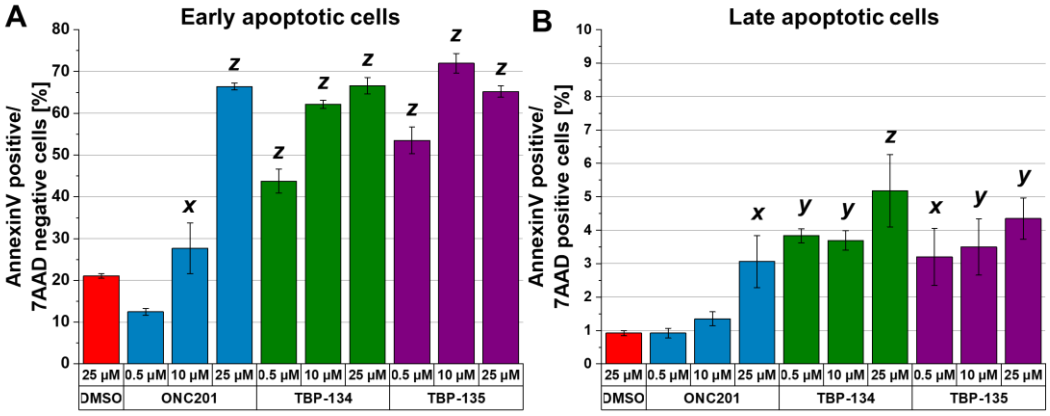

Figure 7. TBP-134 and TBP-135 induced apoptosis after 72-hour treatment at 0.5 µM, whereas ONC201 had no such effect. The ratio of (A) early- and (B) late apoptotic cells normalised to the DMSO control at 72 hours. The data are presented as mean values ± standard deviation (SD) (n=3). Significance levels are shown as x - $p<0.05$; y - $p<0.01$; z - $p<0.001$ using a one-way ANOVA test followed by Fisher's LSD *post hoc* test (71).

The morphometric changes were also monitored to examine the characteristic morphology typical of apoptosis. Three parameters (cell area, optical thickness and optical volume) were observed for 72 hours after treatment. The holographic images excellently indicate changes in morphology, making it easy to detect whether the cells are affected (Figure 8A). In the medium and DMSO controls, the cells appear flat and spread out, represented by dark purple. In contrast, after treatment, the cells are shrunken and rounded, displayed in light yellow. Also, this experiment detected significant differences only after 72 hours of treatment. The average cell area significantly decreased after treatment with 0.5 µM TBP-135 to 338.5 µm^2 (DMSO: 630 µm^2; 1.9-fold) (Figure 8B). While TBP-134 at a higher concentration (25 µM) could exert the same effect, decreased the area to 376 µm^2 (1.7-fold). Both analogues increased the optical thickness at 0.5 µM concentration, TBP-134 increased the parameter to 6.5 µm (DMSO: 1.45 µm; 4.5-fold) and TBP-135 to 5.9 µm (4.1-fold) (Figure 8C). At 0.5 µM, the optical volume of the cells was affected only by TBP-134 treatment, the compound increased the volume to 3112.3 µm^3 (DMSO: 932.5 µm^3; 3.3-fold) (Figure 8D). Meanwhile, ONC201 had no influence on cell morphology at 0.5 µM.

DOI:10.14753/SE.2025.3240

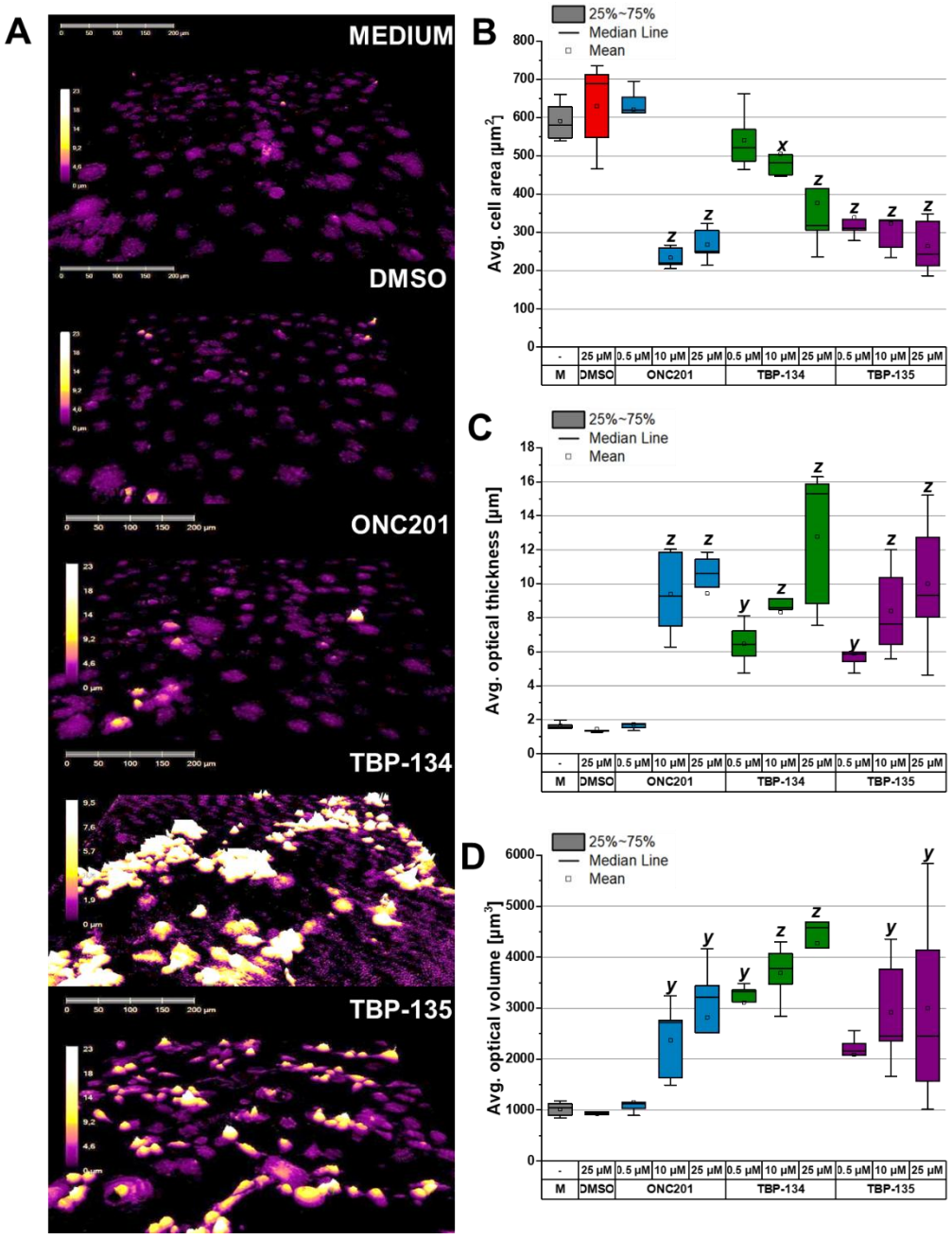

Figure 8. The cells show apoptotic morphology after 72-hour treatment with the fluorinated analogues at 0.5 µM, in contrast to ONC201. (A) The holographic microscopy images of PANC-1 cells after treatment with ONC201, TBP-134, and TBP-135 at 0.5 µM after 72 hours. (B) The average cell area, (C) the average optical thickness and (D) the average optical volume after 72-hour treatment are shown in box charts. The data are presented as mean values ± standard deviation (SD) (n=5). The data were normalised to the DMSO controls. Significance levels are shown as x - $p<0.05$; y - $p<0.01$; z - $p<0.001$ using a one-way ANOVA test followed by Fisher's LSD *post hoc* test (71).

DOI:10.14753/SE.2025.3240

4.1.4. The molecular mechanisms underlying the induced apoptosis

To reveal the molecular players of the induced apoptosis the real-time PCR experiments with ONC201 and its fluorinated derivatives were carried out at earlier time points (3-, 6-, 12-, 24- and 48-hours) on PANC-1 cells. Four target genes (death receptors (*DR4, DR5*), *p53* and *TRAIL*) were chosen to measure the changes in their expression at the RNA level. The expression of *DR4* and *DR5* was increased the most after 24-hour treatment with TBP-135, showing a 3.7-fold and 5.9-fold upregulation, respectively (Figure 9A, B). TBP-134 treatment for 48 hours led to the highest increase in *p53* expression, by 3.7-fold (Figure 9C). Contrary to the literature, ONC201 treatment did not increase the expression of *TRAIL* at any time point, similar results were seen after TBP-134 treatment (Figure 9D). In contrast, TBP-135 treatment caused significant induction in the expression of *TRAIL* after 3 hours, with a 2.4-fold increase.

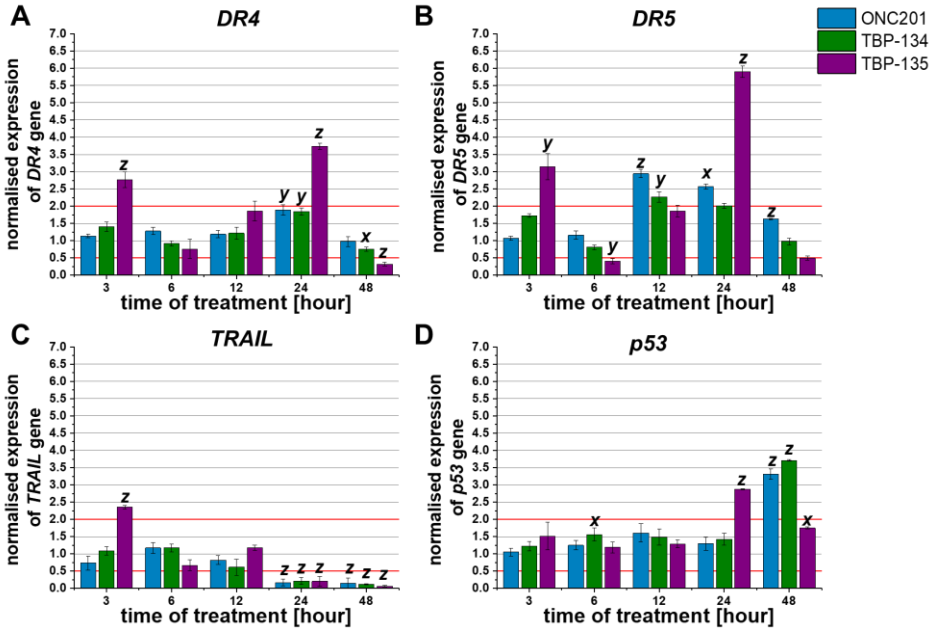

Figure 9. TBP-135 upregulated the expression of *DR4*, *DR5* and *TRAIL* genes, while TBP-134 induced the expression of *p53*. The normalised expression of (A) *DR4*, (B) *DR5*, (C) *p53* and (D) *TRAIL* genes are shown in column charts. The red lines indicate the lower (0.5) and upper (2.0) thresholds of the changes in expression. The data were normalised to the DMSO control. The data are presented as mean values ± standard deviation (SD) (n=3). Significance levels are shown as x - $p<0.05$; y - $p<0.01$; z - $p<0.001$ using a one-way ANOVA test followed by Fisher's LSD *post hoc* test (71).

DOI:10.14753/SE.2025.3240

The protein profile analysis was carried out after a 72-hour treatment with the molecules at 0.5 μM on PANC-1 cells. Out of the 35 tested apoptotic proteins, the relative level of 16 proteins changed significantly (increased or decreased) compared to the DMSO-treated control. Among the 16 proteins, both pro-apoptotic and anti-apoptotic proteins were present. ONC201 treatment increased the levels of multiple pro-apoptotic proteins like cleaved caspase-3, FADD, DR5, SMAC and phospho-p53 (S15, S46, S392) (Figure 10A). While treatment with TBP-135 elevated the levels of DR4, DR5, cleaved and pro-caspase-3, SMAC and phospho-p53 (S15, S46) (Figure 10B). However, after TBP-134 treatment, the levels of DR4 and HSP60 were increased, but the levels of several proteins decreased, like pro-caspase-3, FADD and phospho-p53 (S15, S46, S392) (Figure 10A). The anti-apoptotic protein levels were also influenced following ONC201 treatment, the levels of cIAP-1, HSP60 and XIAP were increased (Figure 10B). Whereas after treatment with the fluorinated analogues, several proteins were undetectable, or their levels were decreased (Figure 10B).

DOI:10.14753/SE.2025.3240

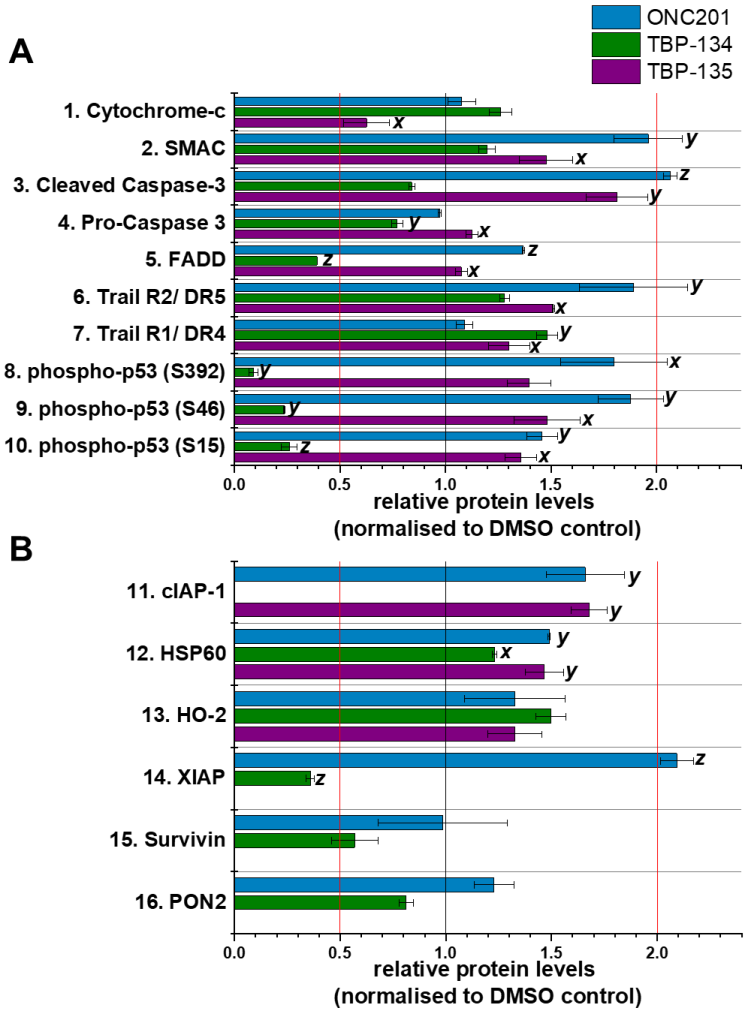

Figure 10. ONC201 and TBP-135 cause similar changes in the apoptotic protein profile compared to TBP-134. The relative (A) pro- and (B) anti-apoptotic protein levels are shown in bar charts. The data were normalised to the DMSO control. The red dashed lines indicate the lower (0.5) and upper (2.0) thresholds of the protein level. The data are presented as mean values ± standard deviation (SD). Significance levels are shown as x - $p<0.05$; y - $p<0.01$; z - $p<0.001$ using a one-way ANOVA test followed by Fisher's LSD *post hoc* test (71).

DOI:10.14753/SE.2025.3240

The functionality of the effector caspases was detected following ONC201 and TBP-135 treatment with a kinetic assay for 72 hours with a fluorescent automated microscope, Celldiscoverer 7 (Figure 11A). The drugs' time-dependent effects were seen in this experiment. Both molecules exerted the best effect after 72-hour treatment. At 0.5 µM, TBP-135 increased the number of caspase-3/7 active cells from 23 (detected in the medium control) to 180 (7.8-fold), while ONC201 increased them to 152 (6.6-fold) (Figure 11B).

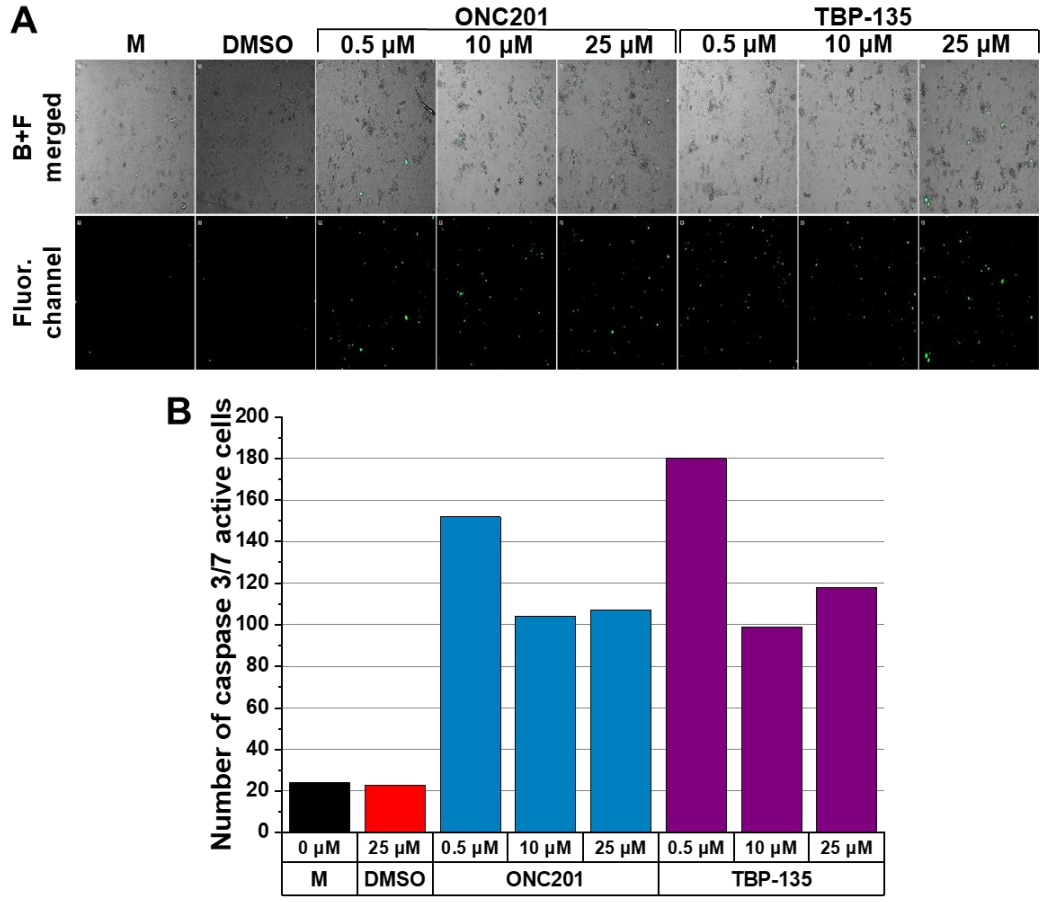

Figure 11. ONC201 and TBP-135 induced caspase-3/-7 activity after 72 hours. (A) The merged brightfield and fluorescent channels and the fluorescent channel images taken with Celldiscoverer 7 at 10x magnification are shown after 72-hour treatment with ONC201 and TBP-135 at 0.5, 10 and 25 µM. The green dots on the images represent the caspase-3/7 active cells. (B) The number of Caspase-3/7 active cells shown in column charts after 72 hours of treatment with ONC201 and TBP-135 (71).

DOI:10.14753/SE.2025.3240

4.1.5. The synergistic effect of ONC201 in combination with bortezomib on A2058 melanoma cells

We determined the synergistic effect of ONC201 and bortezomib on A2058 melanoma cells. We've seen that ONC201 did not have an IC_{50} value on the cell line, however, combined with bortezomib it reduced the effective concentration of bortezomib by approximately half from 23.1 nM to 13.5 nM. This synergistic effect was then revealed on a molecular level. After 72 hours of treatment with ONC201 alone and in combination with bortezomib could increase the expression of DR5 at the protein level in A2058 cells, however, at the same time, the qPCR analysis at the mRNA level showed different tendencies (Table 3) (63). The molecules, either alone or in combination, caused a decrease in the expression of *DR5* at the RNA level after 72 hours of treatment. However, bortezomib alone and in combination with ONC201 (13.5 μM, 40.5 μM) increased the expression of *DR4* by 1.2-fold, 1.4-fold and 1.6-fold, respectively.

Table 3. Bortezomib (BOZ) alone and in combination with ONC201 increased the normalised expression of *DR4* at mRNA level after 72 hours of treatment.

Treatment	normalised gene expression levels	
	DR4	***DR5***
DMSO	0.5 ± 0.04 ^{x}	0.3 ± 0.04 ^{z}
ONC201 13.5 μM	0.1 ± 0.2 ^{z}	0.3 ± 0.2 ^{z}
ONC201 40.5 μM	0.1 ± 0.1 ^{z}	0.5 ± 0.1 ^{z}
BOZ 13.5 nM	1.2 ± 0.1	0.2 ± 0.1 ^{z}
BOZ 13.5 nM + ONC201 13.5 μM	1.4 ± 0.02	0.4 ± 0.02 ^{z}
BOZ 13.5 nM + ONC201 40.5 μM	1.6 ± 0.1 ^{x}	0.5 ± 0.1 ^{z}

The data are presented as mean values ± standard deviation (SD) (n=3). The data were normalised to the medium control. A one-way ANOVA test followed by Fisher's LSD *post hoc* test was used and significance levels are shown as x - $p < 0.05$; y - $p < 0.01$; z - $p < 0.001$ (63).

DOI:10.14753/SE.2025.3240

4.2. The effects of daunorubicin-containing peptide conjugates on PANC-1 cells

4.2.1. GSSEQLYL sequence can successfully target PANC-1 cells

The first step of this study was to select the peptide sequence with the best targeting properties. For this, three sequences were chosen from a paper by Bedi et al. (38). These were GSSEQLYL found in ConjA, ETPPSWGG in ConjB and EPSQSWSM(O) in ConjC. Of the three, only ConjA with the GSSEQLYL targeting peptide showed a viability-reducing effect on PANC-1 cells, it reduced the viability to 8.6% at 10 μM, so it was selected as the parent sequence (Table 4). Next, the position of the amino acid, which can be modified without the loss of the viability-reducing effect, was determined with the help of the so-called Ala-scan. During the Ala-scan, every amino acid in each position is changed to alanin one by one, and their effect on cell viability was measured. The result of this experiment was that in position 6 the amino acid can be changed without the loss of effect, which resulted in Conj03 (targeting sequence: GSSEQAYL). Conj03 had the best effect, at 10 μM it reduced the viability to 14.9%. In position 6, further screening was carried out with numerous coding and non-coding amino acids and halogenated amino acid derivates. After the substitution of Leu^6 with para-chloro-phenylalanine (Conj16 with targeting sequence: GSSEQF(pCl)YL), an anti-tumour effect similar to that of the parent sequence was observed (9.7%). However, other conjugates, such as Conj19 and Conj22, which also contain para-substituted phenylalanine derivatives like Phe(pF) or Phe(pBr), with similar steric properties, were ineffective against PANC-1 cells. Furthermore, substituting with bulky amino acids - such as Phe in Conj09, Asp in Conj13, or Tyr in Conj18 - led to only a slight improvement in overall effectiveness.

In our further studies, based on the viability measurements, the best performing conjugates (ConjA, Conj03 and Conj16) were only investigated and 10 μM was chosen as the used concentration, which demonstrated its effectiveness and suitability for comparison (37).

DOI:10.14753/SE.2025.3240

Table 4. The viability (%) results of PANC-1 cell after 72-hour treatment with 1, 10 and 100 µM conjugates.

Code	Sequence	Group	Viability (%) after 72-hour treatment		
			1 µM	10 µM	100 µM
A	Dau=Aoa-LRRY-GSSEQLYL-NH_2	Conjugates containing original sequence	94.6 ± 3.4	**8.6 ± 1.5^{z}**	0.1 ± 1.3^{z}
B	Dau=Aoa-LRRY-ETPPSWGG-NH_2		104.5 ± 5.1	**139.0 ± 2.1^{z}**	5.7 ± 0.5^{z}
C	Dau=Aoa-LRRY-EPSQSWSM(O)-NH_2		104.7 ± 13.9	**119.4 ± 5.2^{y}**	109.6 ± 1.1
01	Dau=Aoa-LRRY-GSSEQLYA-NH_2	Conjugates from Ala scan	95.4 ± 3.7	**98.7 ± 1.4**	3.8 ± 1.2^{z}
02	Dau=Aoa-LRRY-GSSEQLAL-NH_2		97.2 ± 0.8	**102.9 ± 2.7**	37.7 ± 8.9^{z}
03	Dau=Aoa-LRRY-GSSEQAYL-NH_2		101.2 ± 1.3	**14.9 ± 2.3^{z}**	0 ± 0.9^{z}
04	Dau=Aoa-LRRY-GSSEALYL-NH_2		99.2 ± 1.5	**47.1 ± 3.1^{z}**	0.9 ± 0.9^{z}
05	Dau=Aoa-LRRY-GSSAQLYL-NH_2		93.8 ± 5.5	**93.0 ± 0.5**	11 ± 2.4^{z}
06	Dau=Aoa-LRRY-GSAEQLYL-NH_2		108.3 ± 2	**35.9 ± 5.3^{z}**	2 ± 0.2^{z}
07	Dau=Aoa-LRRY-GASEQLYL-NH_2		96 ± 1.2	**92.9 ± 1.0**	80 ± 15.6^{x}
08	Dau=Aoa-LRRY-ASSEQLYL-NH_2		88.1 ± 4.2^{y}	**53.7 ± 1.1^{z}**	59 ± 2.6^{z}
09	Dau=Aoa-LRRY-GSSEQFYL-NH_2	Conjugates substituted at position 6 by different amino acids or their derivatives	102.6 ± 1.6	**57.3 ± 1.6^{z}**	12 ± 2^{z}
10	Dau=Aoa-LRRY-GSSEQNYL-NH_2		95.9 ± 4	**101.1 ± 2.5**	80.5 ± 10.2^{x}
11	Dau=Aoa-LRRY-GSSEQPYL-NH_2		96.2 ± 6.1	**97.0 ± 5.9**	118.9 ± 4.1^{x}
12	Dau=Aoa-LRRY-GSSEQSYL-NH_2		96.9 ± 3.3	**96.1 ± 7.2**	124.2 ± 3.9^{y}
13	Dau=Aoa-LRRY-GSSEQWYL-NH_2		102.2 ± 5.2	**86.0 ± 3.7^{x}**	0.1 ± 0.2^{z}
14	Dau=Aoa-LRRY-GSSEQIYL-NH_2		102.2 ± 9.4	**105.0 ± 4.6**	44.4 ± 5.8^{z}
15	Dau=Aoa-LRRY-GSSEQNleYL-NH_2		98.7 ± 4.6	**70.8 ± 5.0^{z}**	3.6 ± 0.5^{z}
16	Dau=Aoa-LRRY-GSSEQF(pCl)YL-NH_2		52.6 ± 1.6^{z}	**9.7 ± 1.0^{z}**	0.8 ± 0.9^{z}
17	Dau=Aoa-LRRY-GSSEQEYL-NH_2		92.7 ± 5.1	**135.8 ± 13.5**	58.1 ± 4.6^{z}

18	Dau=Aoa-LRRY-GSSEQYYL-NH_2		83.2 ± 4.5 ^{y}	**48.7 ± 1.6^{z}**	19 ± 1.2^{z}
19	Dau=Aoa-LRRY-GSSEQF(pF)YL-NH_2		97.3 ± 5.1	**108.3 ± 3.6**	16.6 ± 5.4^{z}
20	Dau=Aoa-LRRY-GSSEQF(pMe)YL-NH_2		88.1 ± 7.5 ^{x}	**47.8 ± 8.6^{z}**	68.8 ± 5.6^{z}
21	Dau=Aoa-LRRY-GSSEQF(pOMe)YL-NH_2		99.9 ± 0.4	**105.2 ± 7.0**	161.3 ± 15.9^{z}
22	Dau=Aoa-LRRY-GSSEQF(pBr)YL-NH_2		95.5 ± 2.8	**103.0 ± 21.3**	79.4 ± 13.4^{x}
23	Dau=Aoa-LRRY-GSSEQF(pNO_2)YL-NH_2		101.2 ± 1	**121.4 ± 0.7**	140 ± 8.3^{y}
24	Dau=Aoa-LRRY-GSSEQF(m,mF_2)YL-NH_2		95.6 ± 11.2	**108.5 ± 22.1**	66.4 ± 10.3^{z}
25	Dau=Aoa-LRRY-GSSEQGYL-NH_2		95.8 ± 8.9	**94.9 ± 19.5**	159.6 ± 7.8^{z}
26	Dau=Aoa-LRRY-GSSEQRYL-NH_2		94.5 ± 3.8	**94.8 ± 3.0**	4.2 ± 0.2^{z}

Aoa - aminooxyacetic acid, F(pCl): para-chloro-phenylalanine, F(pF): para-fluoro-phenylalanine, F(pMe): para-methyl-phenylalanine, F(pOMe): para-methoxy-phenylalanine, F(pBr): para-bromo-phenylalanine, F(pNO2): para-nitro-phenylalanine, F(m,mF2): meta, meta-difluoro-phenylalanine. Conjugates with best cytotoxic effect in PANC-1 are highlighted in red. Data were normalised to the medium control. The data shown represent the mean ± SD of three parallels. A one-way ANOVA test followed by Fisher's LSD *post hoc* test was used and significance levels are shown as x - $p < 0.05$; y - $p < 0.01$; z - $p < 0.001$ (59).

Direct cellular cytotoxicity was assessed after 48- and 72-hours of treatment with the conjugates (ConjA, Conj03 and Conj16) and Dau. After 48 hours, neither conjugates caused direct cytotoxicity at 10 µM. In contrast, at 100 µM they all induced a significant direct cytotoxic effect, which was further amplified after 72 hours. At 72 hours, Conj16 at 100 µM (51.9%) nearly achieved the same cytotoxic effect as 10 µM Dau (55.3%). At a concentration of 10 µM, the cytotoxicity % resulting from ConjA (19.8%) and Conj03 (16.0%) treatments remained comparable to the medium control (16.3%), whereas Conj16 increased direct cellular cytotoxicity slightly to 24.3% (by 1.5-fold) (Figure 12).

DOI:10.14753/SE.2025.3240

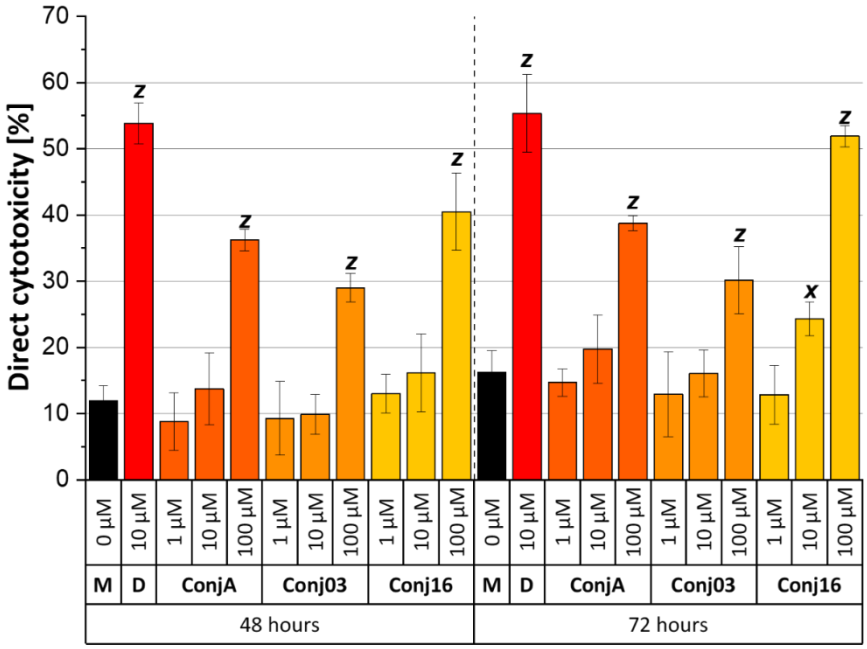

Figure 12. None of the conjugates showed direct cytotoxicity to PANC-1 cells after 48 hours of treatment at 10 µM. Analysis of direct cytotoxicity of the conjugates and daunorubicin (D). The direct cytotoxicity% is determined with the following formula: $cytotoxicity\% = \frac{LDH\ activity_{treated} - LDH\ activity_{spontaneous}}{LDH\ activity_{maximum} - LDH\ activity_{spontaneous}}$ x 100 and was compared to the medium control (M). The data are presented as mean values ± standard deviation (SD) (n = 3). A one-way ANOVA test followed by Fisher's LSD *post hoc* test was used and the levels of significance are shown as x - $p<0.05$; y - $p<0.01$; z - $p<0.001$ (59).

4.2.2. Chlorination enhanced the uptake of the conjugates in PANC-1 cells

To evaluate the cellular uptake of the selected conjugates, ConjA, Conj03 and Conj16, PANC-1 cells were treated with the conjugates at 10 µM and with 0.5 µM Dau serving as a positive control for 1 hour. The fluorescent signal of Dau incorporated in the conjugated or as free form was detected by flow cytometry to quantify the internalization of the conjugates. A primary observation was made that the geometric mean values of the fluorescent intensity for the conjugates were significantly lower compared to the Dau control (Figure 13A, B). This discrepancy in relative fluorescence intensity may be attributed to the conjugation process, as the fluorescence signal of free Dau can decrease upon conjugation with peptides (72).

Despite this reduction, the cells effectively internalised the conjugates (Figure 13B). We hypothesise that the uptake of the conjugates occurs via receptor-mediated endocytosis, whereas Dau enters cells through passive diffusion or the 'flip-flop' mechanism (73). Among the three conjugates tested, the cellular uptake of Conj16 exhibited the highest level (Figure 13A, B).

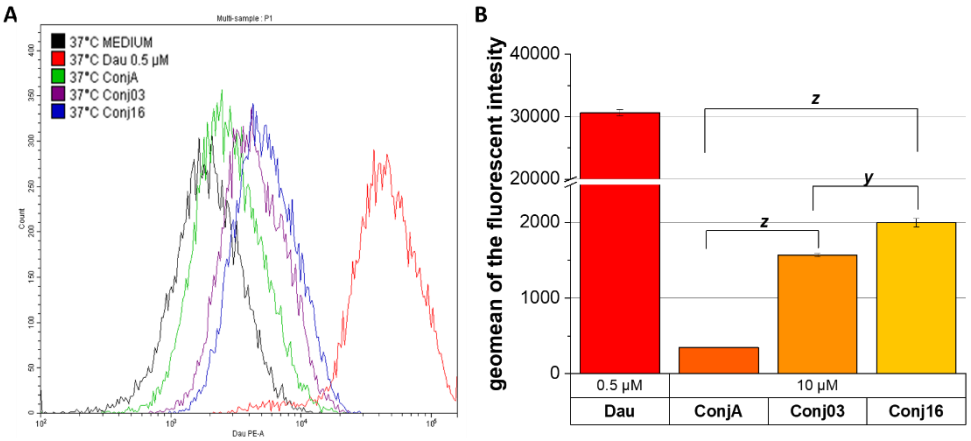

Figure 13. Conj16 was taken up by the cells the most. (A) The histograms represent the fluorescence intensity of the samples treated at 37 °C detected in the phycoerythrin (PE) channel. The medium (black histogram) represents negative control (untreated sample). The Dau (red histogram) represents the internal positive control. (B) The results of the cellular uptake of the conjugates and daunorubicin (Dau) are displayed with the geometric mean (geomean) of the relative fluorescence intensity value normalised to the medium control. One-way ANOVA test followed by Fisher's LSD *post hoc* test was used and the levels of significance are shown as y - $p<0.01$; z - $p<0.001$ (59).

4.2.3. Conj16 induced apoptosis after 48-hour treatment

After 48 hours, Conj16 increased the ratio of late apoptotic cells (AnnexinV positive and To-Pro 3 positive) from 11% to 20% but did not have a significant effect on the ratio of early apoptotic cells (Figure 14A, B). After 72 hours, Conj16 increased the ratio of early apoptotic cells (AnnexinV positive and To-Pro 3 negative) from 1.7% to 9.3% (Figure 14A) and late apoptotic cells from 5.3% to 41.7% (Figure 14B) compared to the medium control. Furthermore, the induction of late apoptosis by Conj16 was comparable to Dau. In contrast, ConjA and Conj03 did not exhibit significant apoptotic effects at either 48 or 72 hours.

DOI:10.14753/SE.2025.3240

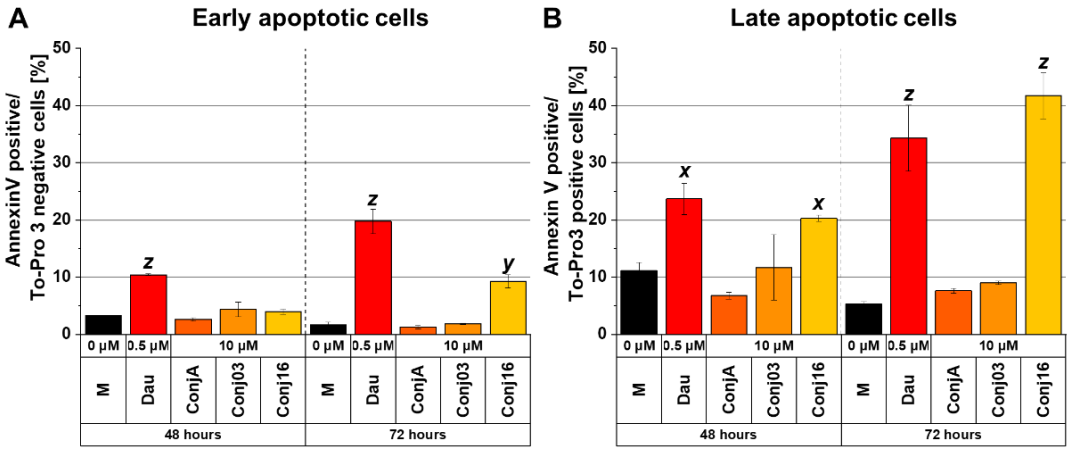

Figure 14. Conj16 induces apoptosis after 48 hours of treatment and this effect is more pronounced after 72 hours. The ratio of (A) early apoptotic (Annexin V positive and To-Pro3 negative) cells and (B) late apoptotic cells (Annexin V and To-Pro3 double positive) is shown after 48- and 72-hour treatment. M stands for medium control. The data normalised to the medium control are presented as mean values ± standard deviation (SD) (n = 3). A one-way ANOVA test followed by Fisher's LSD *post hoc* test was used and the levels of significance are shown as x - $p<0.05$; y - $p<0.01$; z - $p<0.001$ (59).

4.2.4. Conj16 treatment influences the morphology of the cells, showing the characteristic features of cellular senescence

To evaluate the cellular changes such as apoptosis or cellular senescence induced by the conjugates and the free Dau three parameters - average cell area (µm²), average optical thickness (µm) and average optical volume (µm³) - were measured and tracked by HoloMonitor M4 holographic microscope. During apoptosis, as we could see in the 4.1.3 section, there are distinct morphological changes characterised by a decrease in the average cell area and an increase in optical thickness and volume. On the other hand, all three parameters increase during cellular senescence (74, 75).

After 24 hours of treatment with 10 µM Conj16, the morphology of the cells had already significantly changed, which can be seen on the holographic images of the cells (Figure 15).

DOI:10.14753/SE.2025.3240

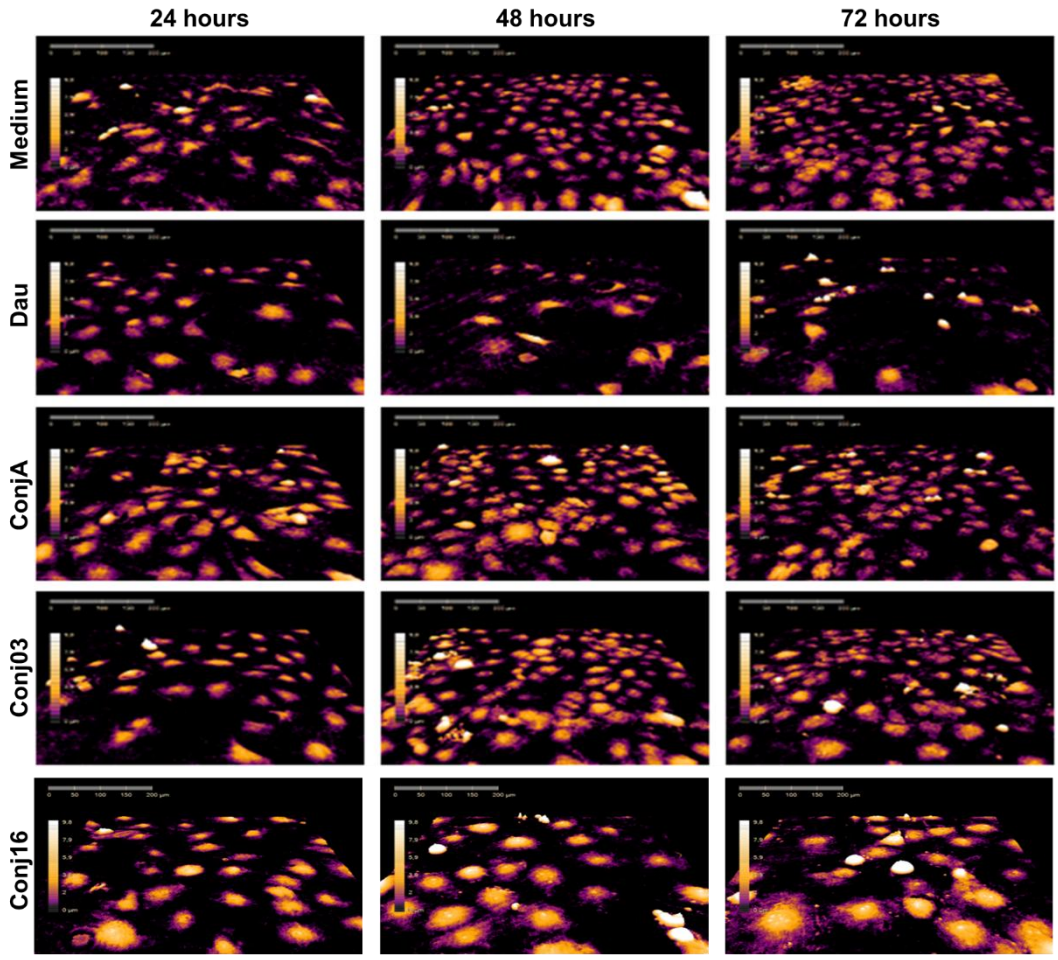

Figure 15. The morphology of the PANC-1 cells have changed already after 24 hours of treatment with Conj16. The holographic microscopy images of PANC-1 cells after treatment with Medium, Dau (0.5 μM), ConjA, Conj03 and Conj16 for 24, 48 and 72 hours (59).

After 24 hours of treatment with Conj16, the average cell area and optical volume increased (Figure 16A, B), while the optical thickness remained unchanged (Figure 16C). After 48 hours, the first two parameters further increased (Figure 16D, E), and the optical thickness was also affected (Figure 16F). However, the most pronounced effect was observed after 72 hours of treatment, resulting in a significant increase in all three parameters monitored: the cell area increased to 2168.8 μm^2 (Medium: 577.7 μm^2, 3.8-fold; Figure 16D), the optical volume increased to 5963.1 μm^3 (Medium: 1001.1 μm^3,6.0-fold; Figure 16E), and the optical thickness increased to 3.0 μm (Medium: 1.6 μm, 1.9-fold; Figure 16F). In contrast, ConjA and Conj03 did not significantly alter cell morphology even after 72 hours (Figure 16G-I).

On the other hand, treatment with 0.5 µM Dau showed different effects. After 48 hours, Dau increased the optical volume to 3505.7 µm^3 (Medium: 1885.6 µm^3, 1.86-fold; Figure 16E) and optical thickness to 2.6 µm (Medium: 1.4 µm, 1.83-fold; Figure 16F) without changing the cell area (Figure 16D). After 72 hours, Dau decreased the cell area to 530.7 µm^2 (0.92-fold; Figure 16G) and further increased the optical volume (2586.5 µm^3) and thickness (5.13 µm) (Figure 16H, I). These results indicate that Dau induces apoptosis as early as 48 hours, whereas Conj16 appears to induce cellular senescence within 24 hours, as reflected in the holographic microscopy images.

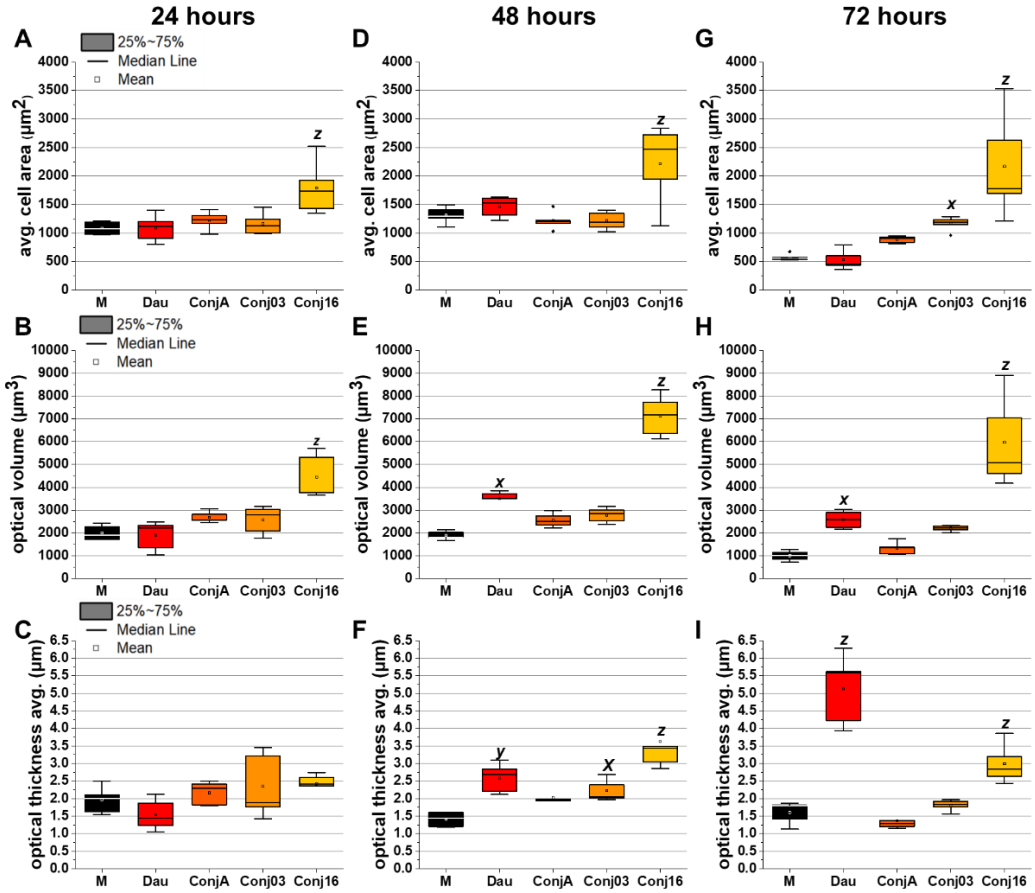

Figure 16. 24 hours of Conj16 treatment reveals that the cells exhibit distinct morphological features associated with cellular senescence. The box charts show the collected data on the (A, D, G) average cell area, (B, E, H) optical volume and (C, F, I) optical thickness average at 24, 48 and 72 hours. M stands for the medium control. The data are presented as mean values ± standard deviation (SD) (n = 5). A one-way ANOVA test followed by Fisher's LSD *post hoc* test was used and the levels of significance are shown as x - $p<0.05$; y - $p<0.01$; z - $p<0.001$ (59).

DOI:10.14753/SE.2025.3240

4.2.5. The molecular background of the cellular senescence induced by Conj16

First, changes in the expression of 88 senescence-related genes were screened using a pre-designed 96-well Bio-Rad PCR plate (Cellular Senescence (SAB Target List) H96). The 48-hour treatment with Conj16 was chosen based on previous results showing that cellular senescence had occurred by this time and apoptosis was not as pronounced. Post-treatment, the expression of 24 genes was upregulated (Figure 17). These upregulated genes were mainly involved in cell cycle regulation, such as *CCNE1*, which increased by 3.1-fold, and strong senescence markers like *CDKN1A* (p21), which increased by 2.2-fold.

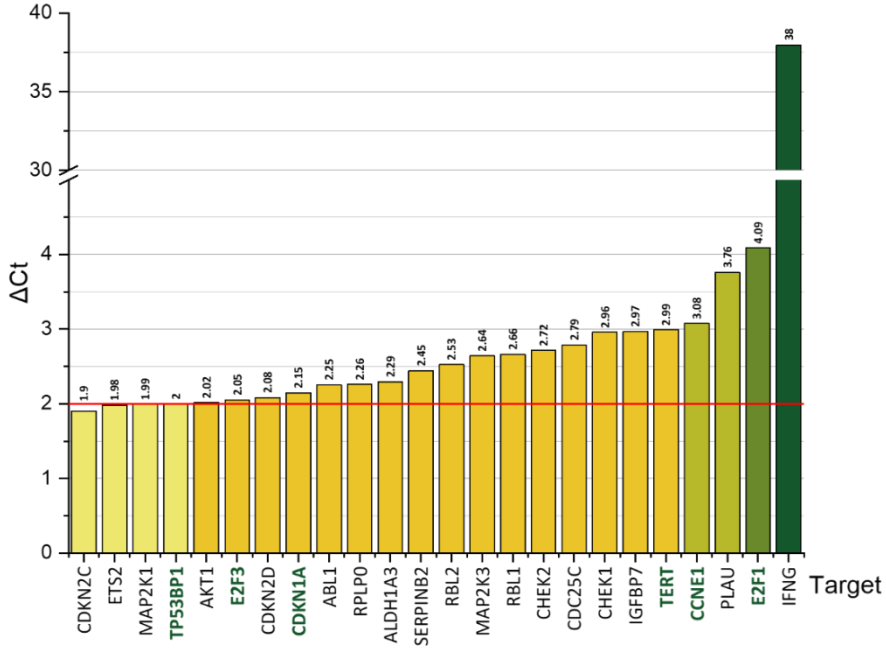

Figure 17. Screening the changes in the expression of senescence-related genes in PANC-1 cells treated with 10 µM Conj16. The reference line indicates the threshold of the changes in expression. The ΔCt values were calculated using the formula: $\Delta Ct = Ct_{medium} - Ct_{Conj16}$ (n = 1) (59).

Based on these findings, 14 genes were selected to compare the senescence-inducing effects of the three conjugates, along with 1 housekeeping gene (*TBP*) for normalizing expression using the $2^{-(\Delta\Delta Ct)}$ method. After 48 hours of treatment with 10 µM Conj16, the expression of *CCNE1*, *CDC25A*, *CDKN1A*, *E2F1*, *E2F2*, and *TERT* was significantly upregulated by more than 2-fold, whereas *CCNA1* expression was downregulated by 0.18-fold (Figure 18). Following treatment with ConjA and

Conj03, the expression of *CCNA1*, *CCNE1*, *CDC25A*, *CDC25C*, and *E2F3* was similarly affected but to varying extents compared to Conj16 (Figure 14B). However, ConjA treatment differed in the expression of *CDKN1A*, *E2F1*, *E2F2*, *GLB1*, *LGALS3* and *TERT* compared to Conj16, because ConjA did not influence the expression of these genes. In contrast, Conj03 treatment did not affect the expression of *CDKN1A*, *E2F1*, *E2F2*, *GLB1*, and *LGALS3* but downregulated *CCND2* by 0.5-fold (Figure 18).

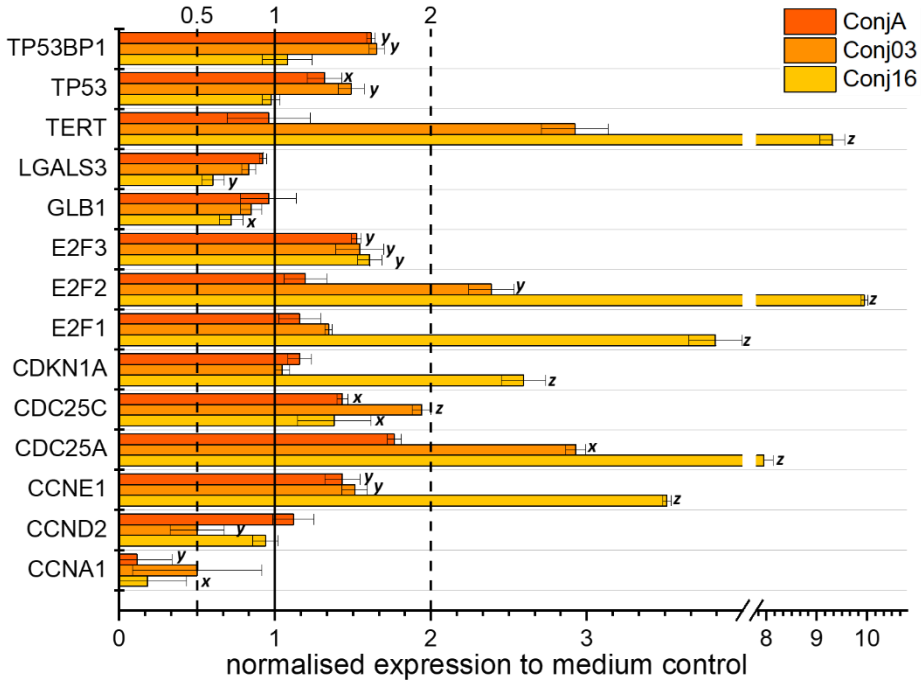

Figure 18. Conj16 treatment increases the expression of a well-known senescence marker, *CDKN1A* (p21), after 48 hours of treatment. The changes in expression of senescence-related genes in PANC-1 cells treated with the conjugates (10 µM). The dashed reference lines indicate the threshold of the changes in expression. The relative expression levels were normalised to the medium control and are presented as mean values ± standard deviation (SD) (n = 3). A one-way ANOVA test followed by Fisher's LSD *post hoc* test was used and the levels of significance are shown as x - $p<0.05$; y - $p<0.01$; z - $p<0.001$ (59).

DOI:10.14753/SE.2025.3240

4.2.6. Treatment with all three conjugates at 10 µM showed no cardiotoxic effects compared to free Dau.

To assess the cardiotoxicity of the conjugates, the viability of HL-1 cardiomyocytes was analysed after 72 hours of incubation with the conjugates. Treatment with the highest concentration of Conj16 (100 µM) and 10 µM Dau reduced cell viability to 3%, while treatment with 100 µM ConjA and Conj03 resulted in cell viability of over 60% (Figure 19). However, after treatment with all three conjugates at 10 µM the viability of HL-1 cells remained over 80%. Notably, 10 µM ConjA decreased viability to a greater extent than 10 µM Conj16 ($p = 0.00072$).

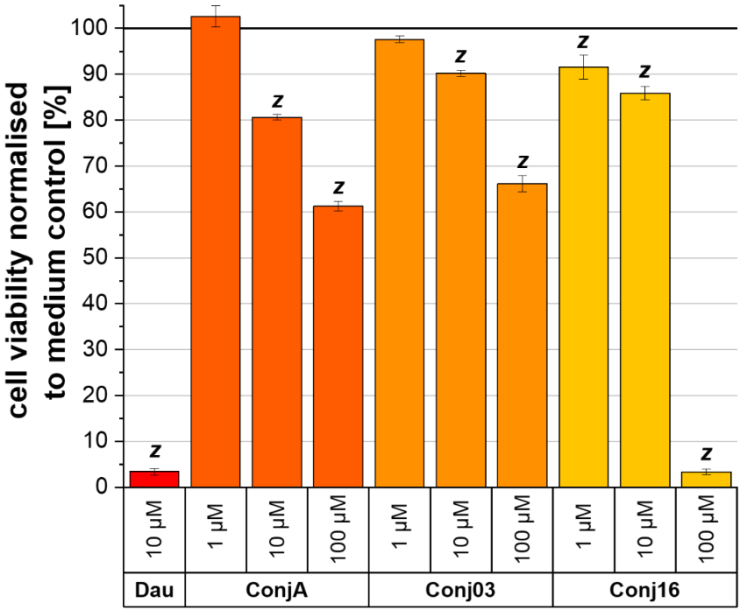

Figure 19. Conjugation with the targeting peptides shows a cardioprotective effect at 1 and 10 µM after 72 hours of treatment. The determination of the cardiotoxic effect of the conjugates and daunorubicin (Dau) on HL-1 cardiomyocyte cell line. The black line indicates the viability of the untreated (medium control) cells. The data normalised to the medium control are presented as mean values ± standard deviation (SD) (n = 3). A one-way ANOVA test followed by Fisher's LSD *post hoc* test was used and the levels of significance are shown as z - $p<0.001$ (59).

DOI:10.14753/SE.2025.3240

5. Discussion

This thesis provided a detailed analysis of the anti-tumour effects of ONC201, its two fluorinated analogues and three daunorubicin-based peptide conjugates designed for targeted therapy on PANC-1 pancreatic ductal adenocarcinoma cells. In both groups of molecules, their anti-tumour potency increased with the introduction of a halogen atom, highlighting the importance of halogenation in enhancing therapeutic efficacy. In the case of the ONC201 analogues, specifically the para-fluorinated analogue, TBP-134, had an IC_{50} value an order of magnitude lower compared to ONC201. Among the three thoroughly investigated PDCs, Conj16, which contains para-chloro-phenylalanine at position 6, demonstrated the highest potency. The significance of these findings is reinforced by broader trends in drug development. In 2021 alone, the Food and Drug Administration approved 14 new halogenated drugs, either fluorinated, chlorinated, or both, demonstrating the widespread acceptance and proven safety of halogenation as a method in drug development (76). This trend highlights the significance and potential implications of the findings in this thesis, as halogen incorporation is not only a widely used strategy but also a proven method for enhancing the pharmacological properties of therapeutic agents (48). The halogenation of molecules can not only enhance the potency of the parent compound but also improve the metabolic stability, allowing the compound to remain in the bloodstream and at the tumour site longer, thereby giving it more time to exert its anti-tumour effects. In addition, halogenation can help prevent chemoresistance, a significant challenge in treating PDAC, which can be either intrinsic or acquired during therapy (77). This dual benefit of enhancing both pharmacokinetic properties and drug potency makes halogenation a valuable strategy in drug design. For instance, fluorination has proven beneficial, as demonstrated by fluoroquinolones. Domagala et al. presented that fluorine introduction at C-6 enhanced the antibacterial activity (78). Similarly, chlorination is demonstrated by clindamycin, a chlorinated derivative of lincomycin, in which the chlorination process improved both absorption and antibacterial effectiveness. Interestingly, halogenation is not limited to lab-developed techniques, as several natural products also contain halogen atoms. Among these, chlorination is more common, with fluorination being less frequently observed in nature (79). For example, the two chlorine atoms in vancomycin (an antibiotic used for multiple-drug-resistant bacteria) are required to achieve its antimicrobial activity (80).

To assess the selectivity and potential side effects of the molecules, normal human dermal fibroblasts were exposed to ONC201 and its analogues. The cardiotoxicity and tumour selectivity of the conjugates were evaluated using the mouse cardiomyocyte cell line HL-1. The findings revealed that ONC201 analogues did not cause cytotoxicity at the concentrations where they demonstrated potent anti-tumour activity against PANC-1 cells, while they showed a slight antiproliferative effect on healthy fibroblasts at much higher concentrations. The conjugates exhibited no cardiotoxicity at a concentration of 10 μM, a level at which the viability of PANC-1 cells was reduced to below 20%. These results underscore the potential of conjugation to alleviate the cardiotoxicity associated with Dau while successfully targeting tumours through the peptide sequence. It aligns with the previous results of our group, which demonstrated the cardioprotective effects of conjugation with GnRH-based peptides (46). These findings indicate that both families of molecules can effectively target tumour cells. However, targeting pancreatic cancers is particularly challenging, as evidenced by the limited availability of targeted therapies. Currently, the only approved treatment is olaparib, which is indicated for patients with BRCA mutations, as mentioned in the introduction (7). Unfortunately, BRCA mutations are relatively uncommon in cases of PDAC, meaning that only a small number of patients can benefit from this therapy (19). In contrast, ONC201 and its analogues could be used in a broader range of cases, not limited to the presence of a single marker.

Despite the successful targeting of PANC-1 cells by these drugs, the two groups of molecules exert their anti-tumour effects differently on the pancreas adenocarcinoma cells. ONC201 and its fluorinated analogues primarily induce cell cycle arrest, leading to apoptosis (Figure 20). After 72 hours of treatment, neither molecule induced direct cytotoxicity. The direct cytotoxicity may suggest potential inflammation post-treatment, which could be linked to various side effects, and it can contribute to the development of metastasis (81, 82). These compounds began to exhibit their anti-tumour effects after 48 hours, with 0.5 μM TBP-134 causing G2/M phase arrest, while 0.5 μM TBP-135 halted the cell cycle in the G1 phase. In contrast, ONC201 did not affect the cell cycle of PANC-1 cells at this concentration and time point. The cell cycle arrest was followed by the induction of apoptotic cell death, with the most significant effects observed after 72 hours of treatment with both analogues, where most cells were found in the early apoptotic stage. These results were further supported by an analysis of morphological changes using

holographic microscopy, which revealed distinct characteristics indicative of apoptosis, with decreased cell area, increased optical thickness and volume. The molecular background of the induced apoptosis was also revealed, suggesting that TBP-135 could induce both the extrinsic and the intrinsic pathways of apoptosis similarly to ONC201. The activation of the extrinsic pathway primarily occurs through the increased expression of DR5. Moreover, TBP-135 and ONC201 not only increased the expression of cleaved caspase-3 after 72 hours of treatment at the protein level, but also they could elevate the number of caspase-3/7 active cells as well. Notably, just after 3 hours of treatment, TBP-135 significantly elevated *TRAIL* expression at the RNA level, in contrast to ONC201. In comparison, TBP-134 appears to primarily activate the intrinsic pathway. While there may be slight activation of the extrinsic pathway, it occurs to a much lesser extent and through DR4.

These differences in activating the apoptotic pathways emphasize the opportunity for selective targeting, which is highly relevant for novel anti-tumour therapies focusing on triggering apoptosis through either the extrinsic or intrinsic pathways (83). Previously, human recombinant TRAIL (dulanermin) was investigated for activating the extrinsic pathway via the death receptors. It was tested in clinical trials combined with modified FOLFOX6 and bevacizumab for treating metastatic colorectal cancer, although the clinical efficacy was not yet defined (84). However, there is evidence that resistance to the treatment may develop (85, 86).

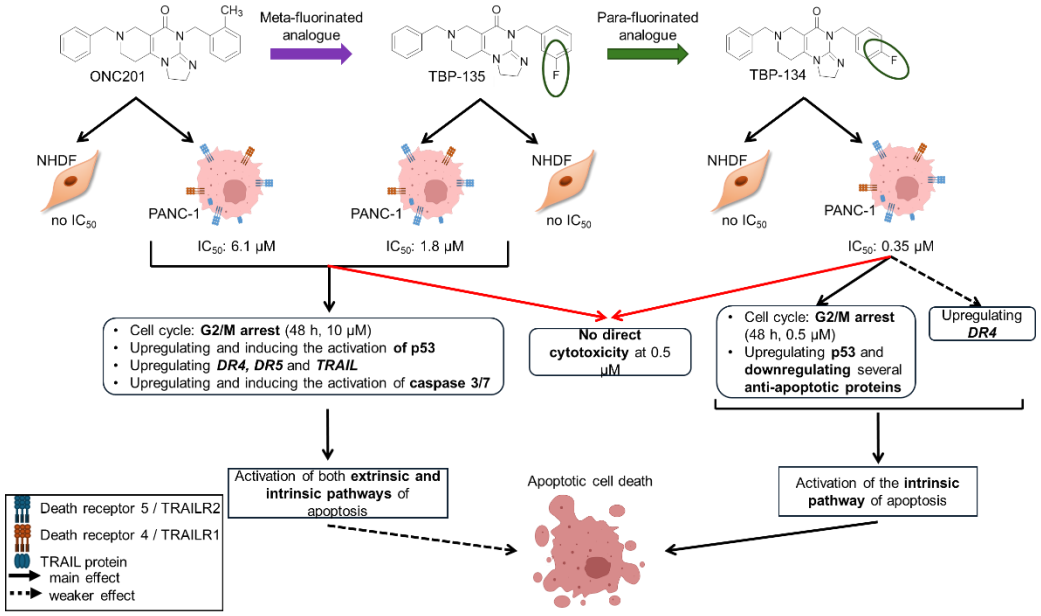

Figure 20. The schematic summary of the effect of ONC201 and its fluorinated analogues on PANC-1 and NHDF cell lines (71).

This thesis also demonstrated that ONC201, in combination with bortezomib, act synergistically on metastatic melanoma A2058 cells. The binary combination of the two molecules enhanced the expression of *DR4* at the RNA level after 72 hours of treatment. However, this result is not in line with the detection of the death receptors at the protein level (63). Moreover, we demonstrated the molecular basis underlying the synergism between ONC201 and bortezomib, likely mediated through DR5 (63). This discrepancy in the mRNA and protein levels of the death receptors may suggest that the increased level of DR5 was not transcriptionally induced. In addition, Zhang et al. reported that ONC201 could sensitize PANC-1 cells to gemcitabine (25). This finding opens up the possibility that the fluorinated analogues of ONC201, which have already demonstrated increased potency and stability, could also serve as sensitizers to gemcitabine in PANC-1 cells or could act synergistically with bortezomib in A2058 cells. By potentially lowering the required dose of gemcitabine, these analogues could reduce the drug's toxicity and improve patient outcomes.

The second half of the thesis focused on revealing the underlying mechanism behind the anti-tumour effects of Dau-containing peptide conjugates (Figure 21). These peptide conjugates can serve as a proficient drug delivery system that can transport the anticancer agents precisely to the tumour cells (87). In our study, firstly, three peptides were conjugated to Dau and screened leading to the identification of ConjA, with the GSSEQLYL sequence, as the most effective conjugate in reducing the viability of PANC-1 cells. The peptide sequence at position 6 is freely modifiable, as revealed by the Ala-scan, leading to the development of Conj03. By introducing a chlorinated amino acid derivate at position 6 (Conj16), the anti-tumour effect was further improved. To determine how this modification might impact safety and to predict the potential inflammatory effects, the direct cytotoxicity was assessed on PANC-1 cells after 48- and 72-hour treatment. After 48 hours, neither conjugate caused direct cytotoxicity to PANC-1 cells, indicating that they may not induce inflammation. However, after 72 hours, Conj16 at 10 μM increased cytotoxicity by 1.5-fold compared to the medium control. The beneficial effect of the modification with chlorinated phenylalanine was also shown in the other measurement. For example, the uptake of the conjugates by the cells was enhanced with the introduction of chlorine. After 1 hour of treatment, Conj16 was internalised by the cells the greatest among the three conjugates. After 48 hours of

treatment, only Conj16 could induce apoptotic cell death, which enhanced further after 72 hours, with cells predominantly found in the late apoptotic stage. Holographic microscopy revealed that just after 24 hours of treatment, Conj16 altered the morphology of PANC-1 cells, showing signs of cellular senescence, which effect was even more noticeable after 48 hours. While ConjA and Conj03 did not affect the morphology, Dau treatment led to apoptotic morphological changes. The molecular basis of the induced senescence by Conj16 likely stems from the increased expression of *CDKN1A/* p21 and the decreased level of *CCNA1* at the RNA level. The protein CDKN1A/p21 is a well-known cellular senescence marker, which is activated in the early stages of senescence (88). Its role is to stably arrest the cell cycle in either G1 or G2 phase in the presence of DNA damage, without the ability to return to the cell cycle program (89). CCNA1 facilitates cell cycle progression, particularly the transition from the G1 to the S phase, when it forms a complex with CDK2 (90). This senescence, triggered by the conjugate, can effectively and permanently arrest the cell cycle, thereby inhibiting the proliferation of tumour cells.

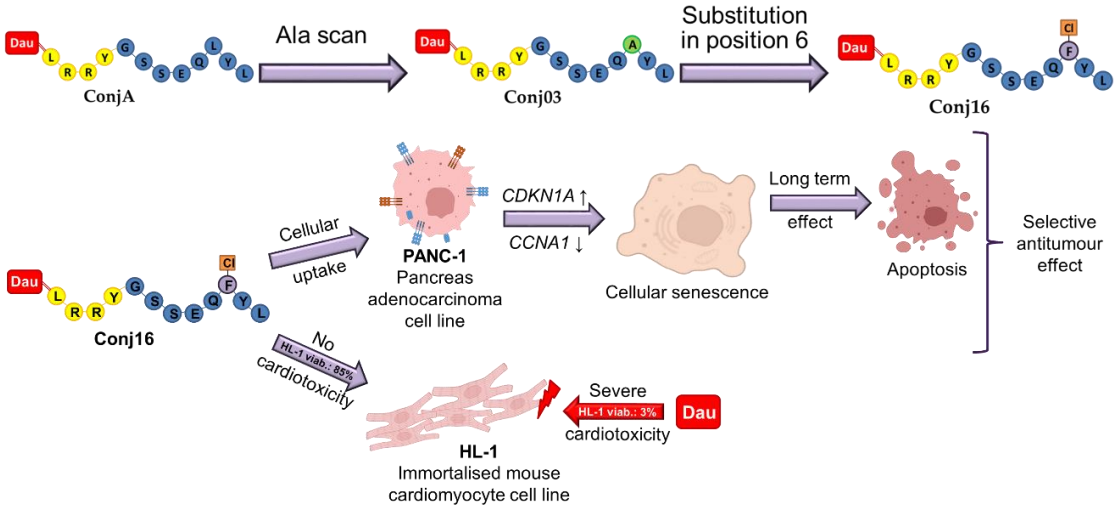

Figure 21. Graphical summary showing the impact of Conj16 on PANC-1 and HL-1 cells. An upward arrow (↑) denotes increased gene expression, while a downward arrow (↓) denotes decreased gene expression. The abbreviation 'HL-1 viab.' refers to the viability of HL-1 cells following a 72-hour treatment with either 10 µM Conj16 or daunorubicin (Dau) (59). The abbreviations found on the figure: *CDKN1A* – p21, *CCNA1* – cyclin A1.

Ultimately, both the small molecules and the peptide-drug conjugates induced programmed cell death, specifically apoptosis, in PANC-1 cells. Apoptosis is a highly desirable form of tumour cell death because it minimises inflammation, unlike necrosis, which often leads to secondary inflammatory responses that can contribute to additional complications (82). This controlled form of cell death allows the body to efficiently remove the apoptotic bodies without causing widespread tissue damage or triggering excessive immune responses (91).

This thesis presented two promising approaches for targeting PDAC: small molecules and peptide-drug conjugates. In both cases, halogenation significantly enhanced the compounds' anti-tumour activity. While each group of molecules has its advantages and disadvantages, they both show strong potential as candidates for further research. Nonetheless, these findings offer substantial hope for the development of novel targeted therapies for PDAC patients, who currently have few effective treatment options. This research aligns with the broader trend in oncology, where personalised and targeted therapies are increasingly being developed to improve patient outcomes (92). Further preclinical studies, including *in vivo* models will be necessary to fully realize the potential of these halogenated compounds. Additionally, exploring combination therapies with existing treatments like gemcitabine could further enhance the therapeutic efficacy of these candidates.

DOI:10.14753/SE.2025.3240

6. Conclusion

This thesis has shown that the fluorinated ONC201 analogues exert a superior anti-tumour effect compared to ONC201, and it also highlights the tumour-targeting and anti-tumour effects of daunorubicin-based peptide conjugates on PANC-1 cells.

- ONC201 and its meta- and para-fluorinated analogue exert potent anti-tumour effects on PANC-1 cells with IC_{50} values ranging from 0.35-6.1 μM.
    a) The analogues not only act as potent anti-tumour agents on the PANC-1 cells, but they also spare the healthy fibroblast cells.
    b) They did not cause direct cytotoxicity after 72 hours of treatment at 0.5 μM.
    c) TBP-134 at 0.5 μM caused G2/M phase arrest in the cell cylce of PANC-1 cells after 48-hour treatment, while TBP-135 halted the cell cycle in G1 phase.
    d) Both fluorinated analogues successfully induced apoptosis after 72 hours of treatment at 0.5 μM, as evidenced by the holographic images as well.
    e) TBP-135 induced the expression of TRAIL at the RNA level after 3 hours of treatment, while ONC201 and TBP-134 did not affect the expression.
    f) TBP-135 activated both the extrinsic and intrinsic pathways similarly to ONC201, while TBP-134 predominantly activated the intrinsic pathway.
    g) ONC201, in combination with bortezomib, could significantly increase the expression of *DR4* at the RNA level in metastatic melanoma A2058 cells.
- The daunorubicin-based peptide conjugates can successfully deliver Dau to PANC-1 cells and deploy the anti-tumour effect of the drug.
    a) The sequence found in ConjA (GSSEQLYL) had the best effect on lowering the viability of PANC-1 cells.
    b) The amino acid in the targeting sequence at position 6 can be freely changed without losing the anti-tumour effect, resulting in Conj03.

Conj16, with para-chlorinated phenylalanine found in position 6, showed the most potent anti-tumour effect out of 18 screened PDCs.

c) After 48 hours of treatment at 10 μM, neither conjugate caused direct cytotoxicity to PANC-1 cells.
d) Conj16 was most efficiently taken up by the cancer cells, showing signs of senescence at both the cell morphological and molecular levels, characterised by increased *CDKN1A* and decreased *CCNA1* mRNA levels, and inducing subsequent apoptotic cell death.
e) The conjugates exhibited no cardiotoxicity at 10 μM in vitro, whereas Dau induced it severely.

DOI:10.14753/SE.2025.3240

7. Summary

Pancreatic ductal adenocarcinoma (PDAC) has a 5-year survival rate of approximately 11%. This poor prognosis is paired with the lack of available targeted therapy treatment options. Therefore, this thesis explores the anti-tumour effects of ONC201, its fluorinated analogues, and daunorubicin-containing peptide conjugates on the PANC-1 PDAC cell line. Furthermore, the thesis also presents the synergistic effect of ONC201 in combination with bortezomib on the A2058 melanoma cell line.

The research shows that adding fluorine and chlorine atoms significantly enhances the potency of the compounds. The thesis reveals that the para-fluorinated ONC201 analogue, TBP-134, had an IC_{50} value of 0.35 μM, much lower than ONC201's 6.1 μM. Among the peptide-drug conjugates (PDC), Conj16 with para-chloro-phenylalanine was the most effective. The compounds were also assessed for selectivity and safety: ONC201 analogues had minimal antiproliferative effects on healthy fibroblasts and no cytotoxicity at effective concentrations, while the conjugates showed no cardiotoxicity at 10 μM. This selective targeting of tumour cells over healthy enhances the therapeutic index and reduces potential side effects.

Additionally, the thesis examines how these molecules exert their anti-tumour effects. ONC201 and its analogues induce apoptosis through different mechanisms. Specifically, both ONC201 and TBP-135 activate apoptosis via both the extrinsic pathway through DR5 and the intrinsic pathway, while TBP-134 predominantly triggers the intrinsic pathway of apoptosis. Moreover, ONC201 could act synergistically through DR5 with bortezomib on A2058 cells, suggesting that the analogues may have the same effect. Conj16, with its chlorinated amino acid, demonstrated increased cellular uptake, induction of cellular senescence and as well as the ability to induce apoptosis. The senescent state was achieved through the downregulation of *CCNA1* and upregulation of *CDKN1A*.

In conclusion, the thesis presents two promising approaches for targeting PDAC: small molecules and PDCs, both improved by halogenation. These findings offer significant hope for developing more effective, targeted therapies for PDAC, a disease with few current treatment options. The research aligns with the broader trend in oncology towards personalised and targeted therapies.

8. References

1. Klein AP. Pancreatic cancer epidemiology: understanding the role of lifestyle and inherited risk factors. Nature Reviews Gastroenterology & Hepatology. 2021;18(7):493-502.

2. Bengtsson A, Andersson R, Ansari D. The actual 5-year survivors of pancreatic ductal adenocarcinoma based on real-world data. Scientific Reports. 2020;10(1):16425.

3. Sherman MH, Beatty GL. Tumor Microenvironment in Pancreatic Cancer Pathogenesis and Therapeutic Resistance. Annual review of pathology. 2023;18:123-48.

4. Stoffel EM, Brand RE, Goggins M. Pancreatic Cancer: Changing Epidemiology and New Approaches to Risk Assessment, Early Detection, and Prevention. Gastroenterology. 2023;164(5):752-65.

5. Shi C, Hong SM, Lim P, Kamiyama H, Khan M, Anders RA, et al. KRAS2 mutations in human pancreatic acinar-ductal metaplastic lesions are limited to those with PanIN: implications for the human pancreatic cancer cell of origin. Molecular cancer research : MCR. 2009;7(2):230-6.

6. Principe DR, Underwood PW, Korc M, Trevino JG, Munshi HG, Rana A. The Current Treatment Paradigm for Pancreatic Ductal Adenocarcinoma and Barriers to Therapeutic Efficacy. Frontiers in oncology. 2021;11:688377.

7. Chi J, Chung SY, Prasad S, Saif MW. The Role of Olaparib in Metastatic Pancreatic Cancer. Cancer medicine journal. 2021;4(3):89-91.

8. Sterner RC, Sterner RM. CAR-T cell therapy: current limitations and potential strategies. Blood Cancer Journal. 2021;11(4):69.

9. Czaplicka A, Lachota M, Pączek L, Zagożdżon R, Kaleta B. Chimeric Antigen Receptor T Cell Therapy for Pancreatic Cancer: A Review of Current Evidence. 2024;13(1):101.

10. Saiki Y, Hirota S, Horii A. Attempts to remodel the pathways of gemcitabine metabolism: Recent approaches to overcoming tumours with acquired chemoresistance. Cancer drug resistance (Alhambra, Calif). 2020;3(4):819-31.

11. Zhao X, Li Z, Gu Z. A new era: tumor microenvironment in chemoresistance of pancreatic cancer. Journal of cancer science and clinical therapeutics. 2022;6(1):61-86.

12. Carvalho TMA, Di Molfetta D, Greco MR, Koltai T, Alfarouk KO, Reshkin SJ, et al. Tumor Microenvironment Features and Chemoresistance in Pancreatic Ductal

Adenocarcinoma: Insights into Targeting Physicochemical Barriers and Metabolism as Therapeutic Approaches. 2021;13(23):6135.

13. Choodetwattana P, Proungvitaya S, Jearanaikoon P, Limpaiboon T. The Upregulation of OCT4 in Acidic Extracellular pH is Associated with Gemcitabine Resistance in Cholangiocarcinoma Cell Lines. Asian Pacific journal of cancer prevention : APJCP. 2019;20(9):2745-8.

14. Randazzo O, Papini F, Mantini G, Gregori A, Parrino B, Liu DSK, et al. "Open Sesame?": Biomarker Status of the Human Equilibrative Nucleoside Transporter-1 and Molecular Mechanisms Influencing its Expression and Activity in the Uptake and Cytotoxicity of Gemcitabine in Pancreatic Cancer. Cancers. 2020;12(11).

15. Jia Y, Xie J. Promising molecular mechanisms responsible for gemcitabine resistance in cancer. Genes & Diseases. 2015;2(4):299-306.

16. Chakkera M, Foote JB, Farran B, Nagaraju GP. Breaking the stromal barrier in pancreatic cancer: Advances and challenges. Biochimica et Biophysica Acta (BBA) - Reviews on Cancer. 2024;1879(1):189065.

17. Liang C, Shi S, Meng Q, Liang D, Ji S, Zhang B, et al. Complex roles of the stroma in the intrinsic resistance to gemcitabine in pancreatic cancer: where we are and where we are going. Experimental & molecular medicine. 2017;49(12):e406.

18. Goulooze SC, Cohen AF, Rissmann R. Olaparib. British journal of clinical pharmacology. 2016;81(1):171-3.

19. Lai E, Ziranu P, Spanu D, Dubois M, Pretta A, Tolu S, et al. BRCA-mutant pancreatic ductal adenocarcinoma. British journal of cancer. 2021;125(10):1321-32.

20. Zhong L, Li Y, Xiong L, Wang W, Wu M, Yuan T, et al. Small molecules in targeted cancer therapy: advances, challenges, and future perspectives. Signal Transduction and Targeted Therapy. 2021;6(1):201.

21. Protein Kinase Inhibitors. LiverTox: Clinical and Research Information on Drug-Induced Liver Injury. Bethesda (MD): National Institute of Diabetes and Digestive and Kidney Diseases; 2012.

22. Kannaiyan R, Mahadevan D. A comprehensive review of protein kinase inhibitors for cancer therapy. Expert review of anticancer therapy. 2018;18(12):1249-70.

23. Stein MN, Bertino JR, Kaufman HL, Mayer T, Moss R, Silk A, et al. First-in-Human Clinical Trial of Oral ONC201 in Patients with Refractory Solid Tumors. Clinical

cancer research : an official journal of the American Association for Cancer Research. 2017;23(15):4163-9.

24. Atkins SLP, Greer YE, Jenkins S, Gatti-Mays ME, Houston N, Lee S, et al. A Single-Arm, Open-Label Phase II Study of ONC201 in Recurrent/Refractory Metastatic Breast Cancer and Advanced Endometrial Carcinoma. The oncologist. 2023;28(10):919-e72.

25. Zhang Q, Wang H, Ran L, Zhang Z, Jiang R. The preclinical evaluation of TIC10/ONC201 as an anti-pancreatic cancer agent. Biochemical and biophysical research communications. 2016;476(4):260-6.

26. Allen JE, Kline CL, Prabhu VV, Wagner J, Ishizawa J, Madhukar N, et al. Discovery and clinical introduction of first-in-class imipridone ONC201. Oncotarget. 2016;7(45):74380-92.

27. Naval J, de Miguel D, Gallego-Lleyda A, Anel A, Martinez-Lostao L. Importance of TRAIL Molecular Anatomy in Receptor Oligomerization and Signaling. Implications for Cancer Therapy. 2019;11(4):444.

28. Monleón I, Martínez-Lorenzo MJ, Anel A, Lasierra P, Larrad L, Piñeiro A, et al. CD59 cross-linking induces secretion of APO2 ligand in overactivated human T cells. European journal of immunology. 2000;30(4):1078-87.

29. Wagner J, Kline CL, Zhou L, Campbell KS, MacFarlane AW, Olszanski AJ, et al. Dose intensification of TRAIL-inducing ONC201 inhibits metastasis and promotes intratumoral NK cell recruitment. The Journal of clinical investigation. 2018;128(6):2325-38.

30. Wang S, Dougan DA. The Direct Molecular Target for Imipridone ONC201 Is Finally Established. Cancer cell. 2019;35(5):707-8.

31. Amoroso F, Glass K, Singh R, Liberal F, Steele RE, Maguire S, et al. Modulating the unfolded protein response with ONC201 to impact on radiation response in prostate cancer cells. Sci Rep. 2021;11(1):4252.

32. Stefanoudakis D, Frountzas M, Schizas D, Michalopoulos NV, Drakaki A, Toutouzas KG. Significance of TP53, CDKN2A, SMAD4 and KRAS in Pancreatic Cancer. Current Issues in Molecular Biology [Internet]. 2024; 46(4):[2827-44 pp.].

33. Bayat Mokhtari R, Homayouni TS, Baluch N, Morgatskaya E, Kumar S, Das B, et al. Combination therapy in combating cancer. Oncotarget. 2017;8(23):38022-43.

34. Coin I, Beyermann M, Bienert M. Solid-phase peptide synthesis: from standard procedures to the synthesis of difficult sequences. Nature Protocols. 2007;2(12):3247-56.

35. Rizvi SFA, Zhang L, Zhang H, Fang Q. Peptide-Drug Conjugates: Design, Chemistry, and Drug Delivery System as a Novel Cancer Theranostic. ACS Pharmacology & Translational Science. 2024;7(2):309-34.

36. Mező G, Gomena J, Ranđelović I, Dókus EL, Kiss K, Pethő L, et al. Oxime-Linked Peptide–Daunomycin Conjugates as Good Tools for Selection of Suitable Homing Devices in Targeted Tumor Therapy: An Overview. 2024;25(3):1864.

37. Dókus LE, Lajkó E, Ranđelović I, Mező D, Schlosser G, Kőhidai L, et al. Phage Display-Based Homing Peptide-Daunomycin Conjugates for Selective Drug Targeting to PANC-1 Pancreatic Cancer. Pharmaceutics. 2020;12(6).

38. Bedi D, Gillespie JW, Petrenko VA. Selection of pancreatic cancer cell-binding landscape phages and their use in development of anticancer nanomedicines. Protein Engineering, Design and Selection. 2014;27(7):235-43.

39. He R, Finan B, Mayer JP, DiMarchi RD. Peptide Conjugates with Small Molecules Designed to Enhance Efficacy and Safety. Molecules (Basel, Switzerland) [Internet]. 2019 2019/05//; 24(10):[E1855 p.]. Available from: http://europepmc.org/abstract/MED/31091786

https://www.mdpi.com/1420-3049/24/10/1855/pdf

https://doi.org/10.3390/molecules24101855

https://europepmc.org/articles/PMC6572008

https://europepmc.org/articles/PMC6572008?pdf=render.

40. Mathews C, Lorusso D, Coleman RL, Boklage S, Garside J. An Indirect Comparison of the Efficacy and Safety of Dostarlimab and Doxorubicin for the Treatment of Advanced and Recurrent Endometrial Cancer. The oncologist. 2022;27(12):1058-66.

41. Aubel-Sadron G, Londos-Gagliardi D. Daunorubicin and doxorubicin, anthracycline antibiotics, a physicochemical and biological review. Biochimie. 1984;66(5):333-52.

42. Minotti G, Sarvazyan N. The anthracyclines: When good things go bad. Cardiovascular Toxicology. 2007;7(2):53-5.

43. Murabito A, Hirsch E, Ghigo A. Mechanisms of Anthracycline-Induced Cardiotoxicity: Is Mitochondrial Dysfunction the Answer? Frontiers in cardiovascular medicine. 2020;7:35.

44. Capranico G, Tinelli S, Austin CA, Fisher ML, Zunino F. Different patterns of gene expression of topoisomerase II isoforms in differentiated tissues during murine development. Biochimica et biophysica acta. 1992;1132(1):43-8.

45. Zhang S, Liu X, Bawa-Khalfe T, Lu L-S, Lyu YL, Liu LF, et al. Identification of the molecular basis of doxorubicin-induced cardiotoxicity. Nature Medicine. 2012;18(11):1639-42.

46. Polgár L, Lajkó E, Soós P, Láng O, Manea M, Merkely B, et al. Drug targeting to decrease cardiotoxicity – determination of the cytotoxic effect of GnRH-based conjugates containing doxorubicin, daunorubicin and methotrexate on human cardiomyocytes and endothelial cells. Beilstein journal of organic chemistry. 2018;14:1583-94.

47. Fu C, Yu L, Miao Y, Liu X, Yu Z, Wei M. Peptide–drug conjugates (PDCs): a novel trend of research and development on targeted therapy, hype or hope? Acta Pharmaceutica Sinica B. 2023;13(2):498-516.

48. Xu Z, Yang Z, Liu Y, Lu Y, Chen K, Zhu W. Halogen Bond: Its Role beyond Drug–Target Binding Affinity for Drug Discovery and Development. Journal of Chemical Information and Modeling. 2014;54(1):69-78.

49. Bauer MR, Jones RN, Baud MGJ, Wilcken R, Boeckler FM, Fersht AR, et al. Harnessing Fluorine–Sulfur Contacts and Multipolar Interactions for the Design of p53 Mutant Y220C Rescue Drugs. ACS chemical biology. 2016;11(8):2265-74.

50. Shah P, Westwell AD. The role of fluorine in medicinal chemistry. Journal of Enzyme Inhibition and Medicinal Chemistry. 2007;22(5):527-40.

51. Chiodi D, Ishihara Y. “Magic Chloro”: Profound Effects of the Chlorine Atom in Drug Discovery. Journal of medicinal chemistry. 2023;66(8):5305-31.

52. Fang WY, Ravindar L, Rakesh KP, Manukumar HM, Shantharam CS, Alharbi NS, et al. Synthetic approaches and pharmaceutical applications of chloro-containing molecules for drug discovery: A critical review. European journal of medicinal chemistry. 2019;173:117-53.

53. Ke N, Wang X, Xu X, Abassi YA. The xCELLigence system for real-time and label-free monitoring of cell viability. Methods in molecular biology (Clifton, NJ). 2011;740:33-43.

54. Martin SJ, Reutelingsperger CP, McGahon AJ, Rader JA, van Schie RC, LaFace DM, et al. Early redistribution of plasma membrane phosphatidylserine is a general feature of apoptosis regardless of the initiating stimulus: inhibition by overexpression of Bcl-2 and Abl. The Journal of experimental medicine. 1995;182(5):1545-56.

55. Li J, Gray BD, Pak KY, Ng CK. Targeting phosphatidylethanolamine and phosphatidylserine for imaging apoptosis in cancer. Nuclear medicine and biology. 2019;78-79:23-30.

56. Martin RM, Leonhardt H, Cardoso MC. DNA labeling in living cells. Cytometry Part A : the journal of the International Society for Analytical Cytology. 2005;67(1):45-52.

57. Zembruski NC, Stache V, Haefeli WE, Weiss J. 7-Aminoactinomycin D for apoptosis staining in flow cytometry. Analytical biochemistry. 2012;429(1):79-81.

58. Tavecchio M, Simone M, Bernasconi S, Tognon G, Mazzini G, Erba E. Multi-parametric flow cytometric cell cycle analysis using TO-PRO-3 iodide (TP3): detailed protocols. Acta histochemica. 2008;110(3):232-44.

59. Szász Z, Enyedi KN, Takács A, Fekete N, Mező G, Kőhidai L, et al. Characterisation of the cell and molecular biological effect of peptide-based daunorubicin conjugates developed for targeting pancreatic adenocarcinoma (PANC-1) cell line. Biomedicine & pharmacotherapy = Biomedecine & pharmacotherapie. 2024;173:116293.

60. Crowley LC, Chojnowski G, Waterhouse NJ. Measuring the DNA Content of Cells in Apoptosis and at Different Cell-Cycle Stages by Propidium Iodide Staining and Flow Cytometry. Cold Spring Harbor protocols. 2016;2016(10).

61. Lajkó E, Spring S, Hegedüs R, Biri-Kovács B, Ingebrandt S, Mező G, et al. Comparative cell biological study of in vitro antitumor and antimetastatic activity on melanoma cells of GnRH-III-containing conjugates modified with short-chain fatty acids. Beilstein journal of organic chemistry. 2018;14:2495-509.

62. Kumar P, Nagarajan A, Uchil PD. Analysis of Cell Viability by the Lactate Dehydrogenase Assay. Cold Spring Harbor protocols. 2018;2018(6).

63. Takács A, Szász Z, Kalabay M, Bárány P, Csámpai A, Hegyesi H, et al. The Synergistic Activity of Bortezomib and TIC10 against A2058 Melanoma Cells. Pharmaceuticals (Basel, Switzerland). 2021;14(8).

64. Sebesta M, Egelberg P, Langberg A, Lindskov J-H, Alm K, Janicke B. HoloMonitor M4: holographic imaging cytometer for real-time kinetic label-free live-cell analysis of adherent cells: SPIE; 2016.

65. Mandavilli BS, Yan M, Clarke S. Cell-Based High Content Analysis of Cell Proliferation and Apoptosis. Methods in molecular biology (Clifton, NJ). 2018;1683:47-57.

66. Livak KJ, Schmittgen TD. Analysis of relative gene expression data using real-time quantitative PCR and the 2(-Delta Delta C(T)) Method. Methods (San Diego, Calif). 2001;25(4):402-8.

67. McCarthy DJ, Smyth GK. Testing significance relative to a fold-change threshold is a TREAT. Bioinformatics (Oxford, England). 2009;25(6):765-71.

68. Brosseau N, Andreev E, Ramotar D. Uptake Assays to Monitor Anthracyclines Entry into Mammalian Cells. Bio-protocol. 2017;7(18):e2555.

69. Zhang P, Cheetham AG, Lock LL, Cui H. Cellular uptake and cytotoxicity of drug-peptide conjugates regulated by conjugation site. Bioconjugate chemistry. 2013;24(4):604-13.

70. Lajkó E, Hegedüs R, Mező G, Kőhidai L. Apoptotic Effects of Drug Targeting Conjugates Containing Different GnRH Analogs on Colon Carcinoma Cells. International journal of molecular sciences. 2019;20(18).

71. Szász Z, Takács A, Kalabay M, Bárány P, Czuczi T, Csámpai A, et al. Comparative study of the anti-tumour effects of the imipridone, ONC201 and its fluorinated analogues on pancreatic cancer cell line. Sci Rep. 2025;15(1):15925.

72. Orbán E, Manea M, Marquadt A, Bánóczi Z, Csík G, Fellinger E, et al. A new daunomycin-peptide conjugate: synthesis, characterization and the effect on the protein expression profile of HL-60 cells in vitro. Bioconjugate chemistry. 2011;22(10):2154-65.

73. Regev R, Yeheskely-Hayon D, Katzir H, Eytan GD. Transport of anthracyclines and mitoxantrone across membranes by a flip-flop mechanism. Biochemical Pharmacology. 2005;70(1):161-9.

74. Saraste A, Pulkki K. Morphologic and biochemical hallmarks of apoptosis. Cardiovascular research. 2000;45(3):528-37.

75. Beck J, Horikawa I, Harris C. Cellular Senescence: Mechanisms, Morphology, and Mouse Models. 2020;57(6):747-57.

76. Benedetto Tiz D, Bagnoli L, Rosati O, Marini F, Sancineto L, Santi C. New Halogen-Containing Drugs Approved by FDA in 2021: An Overview on Their Syntheses and Pharmaceutical Use. Molecules (Basel, Switzerland). 2022;27(5).

77. Grasso C, Jansen G, Giovannetti E. Drug resistance in pancreatic cancer: Impact of altered energy metabolism. Critical Reviews in Oncology/Hematology. 2017;114:139-52.

78. Domagala JM, Hanna LD, Heifetz CL, Hutt MP, Mich TF, Sanchez JP, et al. New structure-activity relationships of the quinolone antibacterials using the target enzyme. The development and application of a DNA gyrase assay. Journal of medicinal chemistry. 1986;29(3):394-404.

79. Neumann CS, Fujimori DG, Walsh CT. Halogenation Strategies In Natural Product Biosynthesis. Chemistry & Biology. 2008;15(2):99-109.

80. Harris CM, Kannan R, Kopecka H, Harris TM. The role of the chlorine substituents in the antibiotic vancomycin: preparation and characterization of mono- and didechlorovancomycin. Journal of the American Chemical Society. 1985;107(23):6652-8.

81. Walker AK, Chan RJ, Vardy JL. Sustained Mild Inflammation in Cancer Survivors: Where to from Here? JNCI cancer spectrum. 2022;6(4).

82. Vyas D, Laput G, Vyas AK. Chemotherapy-enhanced inflammation may lead to the failure of therapy and metastasis. OncoTargets and therapy. 2014;7:1015-23.

83. Carneiro BA, El-Deiry WS. Targeting apoptosis in cancer therapy. Nature reviews Clinical oncology. 2020;17(7):395-417.

84. Wainberg ZA, Messersmith WA, Peddi PF, Kapp AV, Ashkenazi A, Royer-Joo S, et al. A phase 1B study of dulanermin in combination with modified FOLFOX6 plus bevacizumab in patients with metastatic colorectal cancer. Clinical colorectal cancer. 2013;12(4):248-54.

85. Montinaro A, Walczak H. Harnessing TRAIL-induced cell death for cancer therapy: a long walk with thrilling discoveries. Cell Death & Differentiation. 2023;30(2):237-49.

86. Sahu RP, Batra S, Kandala PK, Brown TL, Srivastava SK. The role of K-ras gene mutation in TRAIL-induced apoptosis in pancreatic and lung cancer cell lines. Cancer chemotherapy and pharmacology. 2011;67(2):481-7.

87. Gong L, Zhao H, Liu Y, Wu H, Liu C, Chang S, et al. Research advances in peptide–drug conjugates. Acta Pharmaceutica Sinica B. 2023;13(9):3659-77.

88. Huang W, Hickson LJ, Eirin A, Kirkland JL, Lerman LO. Cellular senescence: the good, the bad and the unknown. Nature Reviews Nephrology. 2022;18(10):611-27.

89. Kumari R, Jat P. Mechanisms of Cellular Senescence: Cell Cycle Arrest and Senescence Associated Secretory Phenotype. 2021;9.

90. Ji P, Agrawal S, Diederichs S, Bäumer N, Becker A, Cauvet T, et al. Cyclin A1, the alternative A-type cyclin, contributes to G1/S cell cycle progression in somatic cells. Oncogene. 2005;24(16):2739-44.

91. Elmore S. Apoptosis: a review of programmed cell death. Toxicologic pathology. 2007;35(4):495-516.

92. Zhou Z, Li M. Targeted therapies for cancer. BMC medicine. 2022;20(1):90.

9. Bibliography of candidate's publications

9.1. List of publications used for the thesis

1. Zsófia Szász, Kata Nóra Enyedi, Angéla Takács, Nóra Fekete, Gábor Mező, László Kőhidai, Eszter Lajkó (2024) Characterisation of the cell and molecular biological effect of peptide-based daunorubicin conjugates developed for targeting pancreatic adenocarcinoma (PANC-1) cell line. Biomedicine & Pharmacotherapy. 173:116293

   IF: 7.5; D1

2. Angéla Takács[#], Zsófia Szász[#], Márton Kalabay, Péter Bárány, Antal Csámpai, Hargita Hegyesi, Orsolya Láng, Eszter Lajkó, László Kőhidai (2021) The Synergistic Activity of Bortezomib and TIC10 against A2058 Melanoma Cells. Pharmaceuticals (Basel). 14(8): 820
   [#] shared first authorship

   IF 5.215; Q1

3. Zsófia Szász[#], Angéla Takács[#], Márton Kalabay, Péter Bárány, Tamás Czuczi, Antal Csámpai, Eszter Lajkó, László Kőhidai (2025) Comparative study of the anti-tumour effects of the imipridone, ONC201 and its fluorinated analogues on pancreatic cancer cell line. Scientific Reports. 15:15925
   [#] shared first authorship

   IF: 3.9; D1

9.2. List of publications not used for the thesis

1. Angéla Takács, Malin Jessen, Eszter Lajkó, Zsófia Szász, Márton Kalabay, Antal Csámpai, László Kőhidai (2025) Quinine-chalcone hybrides as potent inhibitors of P-glycoprotein with apoptotic effects on EBC-1 cells. Biomedicine & Pharmacotherapy. 187:118076

   IF: 7.5; D1

2. Bálint Budavári, Áron Karancsi, Balázs Gábor Pinke, Éva Pállinger, Krisztina Juriga-Tóth, Márton Király, Zsófia Szász, István Voszka, Kolos Molnár, László Kőhidai, Angéla Jedlovszky-Hajdú, Krisztina S. Nagy (2024) Long-term shelf-life liposomes for delivery of prednisolone and budesonide. Journal of Molecular Liquids. 394:123756

   IF: 5.2; Q1

3. Márton Kalabay, Zsófia Szász, Orsolya Láng, Eszter Lajkó, Éva Pállinger, Cintia Duró, Tamás Jernei, Antal Csámpai, Angéla Takács, László Kőhidai (2022) Investigation of the Antitumor Effects of Tamoxifen and Its Ferrocene-Linked Derivatives on Pancreatic and Breast Cancer Cell Lines. Pharmaceuticals (Basel). 15(3):314 15

   IF: 5.215; Q1

4. Kinga Judit Fodor, Dániel Hutai, Tamás Jernei, Angéla Takács, Zsófia Szász, Máté Sulyok-Eiler, Veronika Harmat, Rita Oláh Szabó, Gitta Schlosser, Ferenc Hudecz, László Kőhidai, Antal Csámpai (2020) Novel Polycondensed Partly Saturated β-Carbolines Including Ferrocene Derivatives: Synthesis, DFT-Supported Structural Analysis, Mechanism of Some Diastereoselective Transformations and a Preliminary Study of Their in vitro Antiproliferative Effects. Molecules 25(7):1599

   IF: 4.412; Q1

5. Gábor Mező, Levente Dókus, Gitta Schlosser, Eszter Lajkó, Zsófia Szász, Ivan Randelovic, Beáta Biri-Kovács, József Tóvári, László Kõhidai (2019) Hasnyálmirigytumort célzó terápiás irányítópeptidek összehasonlítása. Magyar Onkológia 63:4

The cumulative impact factor: 38.942

DOI:10.14753/SE.2025.3240

10. Acknowledgements

I want to express my deepest gratitude to my supervisors, Dr. Eszter Lajkó and Prof. Dr. László Kőhidai, whose guidance and support from the very beginning have made this work possible. Their valuable and insightful advice has been essential in preparing and fine-tuning this thesis.

I also want to extend my heartfelt thanks to Dr. Angéla Takács for her work and supervision of my student research work (TDK), which significantly contributed to my pharmacist degree.

Furthermore, I would like to express my appreciation for their help and valuable advice to Dr. Éva Pállinger, Dr. Márton Kalabay, Petra Pőcze, Nóra Fekete, Maja Molnár and Andrea Kovács.

I am also deeply grateful to Prof. Dr. Edit Buzás for enabling me to pursue my studies in the Department of Genetics, Cell- and Immunobiology.

I wish to extend my gratitude to all of my colleagues in the department, especially to Dorina Lenzinger, Zsuzsanna Adamecz, Bence Nagy and András Försönits, who supported me through both the challenges and joyful moments of achieving my goal.

I am sincerely appreciative of the tremendous help and patience of my husband, who has always been supportive. Although my mother and grandmother are no longer with us, I carry their memory in my heart as I complete my PhD - a journey they would have shared with me.